

VIBRATION ISOLATION OF A LOCOMOTIVE MOUNTED
ENERGY STORAGE FLYWHEEL

A Thesis

by

XIAOHUA ZHANG

Submitted to the Office of Graduate Studies of
Texas A&M University
in partial fulfillment of the requirements for the degree of
MASTER OF SCIENCE

December 2009

Major Subject: Mechanical Engineering

VIBRATION ISOLATION OF A LOCOMOTIVE MOUNTED
ENERGY STORAGE FLYWHEEL

A Thesis

by

XIAOHUA ZHANG

Submitted to the Office of Graduate Studies of
Texas A&M University
in partial fulfillment of the requirements for the degree of

MASTER OF SCIENCE

Approved by:

Chair of Committee,	Alan Palazzolo
Committee Members,	Alexander Parlos
	Gary Fry
Head of Department,	Dennis O'Neal

December 2009

Major Subject: Mechanical Engineering

ABSTRACT

Vibration Isolation of a Locomotive Mounted Energy Storage Flywheel.

(December 2009)

Xiaohua Zhang, B.E., Shanghai University, P.R. China

Chair of Advisory Committee: Dr. Alan Palazzolo

Utilizing flywheels to store and reuse energy from regenerative braking on locomotives is a new technology being developed in the Vibration Control and Electromechanics Lab at Texas A&M. This thesis focuses on the motion analysis of a locomotive mounted energy storage flywheel system for a variety of support motion inputs. Two input cases, sinusoidal floor input and ramp input, are analyzed in different sections. Simulation results and methods of ensuring the operating success of the flywheel system are provided at the end of each section.

Section 1 introduces the problem and method being used to study the vibration under different circumstances. Section 2 analyzes the response of the flywheel system to sinusoidal floor input given by Ahmadian and Venezia 2000. Natural frequency and transmissibility of the system are utilized to explain the simulation results carried out in the frequency domain. It is found that the motion differences between flywheels(rotors) and magnetic bearings(stators) are guaranteed to be small. Section 3 emulates the locomotive traversing a bump with 1:150 slope. Simulation shows that catcher(backup) bearings are needed to limit the vibration of rotors through a bump. It is also found that

gyroscopic effect causes problems in vibration isolation. Section 4 explores de-levitation method and installation of gimbals as possible remedies to this problem. Finally, a summary of simulation results from different input cases is made.

To my Mom, Lichun Liu

ACKNOWLEDGEMENTS

This thesis witnesses my progress under Dr. Palazzolo's dedicated guidance. I really appreciate being his student worker for a year. During this year, I learned a lot, from dynamic modeling to vibration analysis. Most importantly, he taught me how to apply the knowledge learned in class to industry and everyday life. His expertise knowledge and experience in engineering highly impressed me and convinced me to further my education under him. I also want to thank Dr. Parlos during my graduate study. His instruction in control is one of the most interesting and understandable I have ever had. Thanks also extend to Dr. Fry. Many of his suggestions will definitely be helpful in future research work. Meanwhile, I am grateful for the help and support that Mr. Iden and Mr. Davis from Association of American Railroads provided during this research. Additionally, I want to express my gratitude to Texas A&M for providing me with an excellent education. I am and will always be proud of being an Aggie.

Finally, all my work owes to my beloved Mom, Lichun Liu. Without her consistent support and encouragement, I would not have arrived at where I am now.

TABLE OF CONTENTS

	Page
ABSTRACT	iii
DEDICATION	v
ACKNOWLEDGEMENTS	vi
TABLE OF CONTENTS	vii
LIST OF FIGURES.....	ix
LIST OF TABLES	xiii
1. INTRODUCTION.....	1
1.1 Problem statement.....	1
1.2 Objective and significance	1
1.3 Literature review	2
2. MOTION ANALYSIS OF SINUSOIDAL INPUT	5
2.1 Introduction	5
2.2 Model setup	5
2.3 Force analysis.....	8
2.4 System properties	12
2.5 Source of input	21
2.6 Simulation results.....	25
3. MOTION ANALYSIS OF RAMP SUPPORT INPUT	29
3.1 Introduction	29
3.2 Model setup	30
3.3 Motion analysis	30
3.4 Model with catcher bearings	37
4. DE-LEVITATION METHOD WITH RAMP INPUT.....	46
4.1 Introduction	46
4.2 Model setup	46

	Page
4.3 Motion analysis	50
4.4 Model with gimbals.....	55
5. SUMMARY	58
REFERENCES.....	60
APPENDIX A	62
APPENDIX B	65
VITA	68

LIST OF FIGURES

FIGURE		Page
1	Model setup	6
2	Model dimensions	6
3	Stack layout	8
4	FBD of housing and rotor.....	9
5	FBD for housing_1	11
6	θ -motion natural frequencies vary with spin velocity	14
7	Transmissibility of z motion	17
8	Transmissibility of θ motion	19
9	Definition of largest relative motion	21
10	Sinusoidal input signals (z, θ_x)	22
11	Relative motion between rotor and housing due to sinusoidal floor input.	25
12	Relative motion due to sinusoidal floor input in vertical direction from AAR's data at $K_{AMB} = 1000$ lbs/in	26
13	Relative motion due to sinusoidal floor input in vertical direction from AAR's data at $K_{AMB} = 250,000$ lbs/in	27
14	Rotors' motion with respect to floor due to sinusoidal floor input in vertical direction from AAR's data at $K_{AMB} = 250,000$ lbs/in.....	27
15	Ramp support input model	29
16	Additional model setup	30

LIST OF FIGURES (CONTINUED)

FIGURE	Page
17 Motion assumption of floor model.....	31
18 Largest relative motion vs. time for ramp input without catcher bearing at 0 rad/sec.....	34
19 Largest relative motion vs. time for ramp input without catcher bearing at 500 rad/sec.....	34
20 Maximum relative motion vs. different stiffness of the 1 st layer isolator ..	35
21 Maximum relative motion vs. different AMB stiffness	36
22 Setup model with catcher bearings.....	37
23 3-D illustration of the model with catcher bearings.....	38
24 Interactive forces on the rotor and housing.....	39
25 Relative motion with catcher bearings (AMB stiffness: 1,000 lbs/in; AMB damping ratio: 0.05; catcher bearing stiffness: 1,000,000 lbs/in; catcher bearing damping: 450 lb sec/in; spin rate: 0rad/sec)	41
26 Relative motion with catcher bearings(AMB stiffness:250,000 lbs/in; AMB damping ratio: 0.05; catcher bearing stiffness: 1,000,000 lbs/in; catcher bearing damping: 450 lb sec/in; spin rate: 0rad/sec)	42
27 1 st layer's absolute motion with catcher bearings(AMB stiffness: 250,000 lbs/in; AMB damping ratio:0.05;spin rate: 0rad/sec) ...	42

LIST OF FIGURES (CONTINUED)

FIGURE	Page
28 Relative motion with catcher bearings (AMB stiffness: 250,000 lbs/in; AMB damping ratio: 0.05; spin rate: 500rad/sec).....	43
29 1 st layer's absolute motions with catcher bearings (AMB stiffness: 250,000lbs/in; AMB damping ratio:0.05;spin rate:500rad/sec) .	43
30 Relative motion with catcher bearings (AMB stiffness: 1,000,000lbs/in; AMB damping ratio: 0.05; spin rate: 500rad/sec).....	44
31 1 st layer's absolute motions with catcher bearings (AMB stiffness: 1,000,000lbs/in; AMB damping ratio: 0.05; spin rate: 500rad/sec).....	44
32 Relative motion with catcher bearings (AMB stiffness: 250,000lbs/in; AMB damping ratio: 0.3; spin rate: 500rad/sec).....	45
33 1 st layer's absolute motions with catcher bearings (AMB stiffness: 1,000,000 lbs/in; AMB damping ratio: 0.3; spin rate: 500 rad/sec).....	45
34 One layer of de-levitation model on yz plane	47
35 Whole model for the simulation.....	48
36 De-levitation without downward magnetic forces at 0rad/sec spin rate	53
37 De-levitation without downward magnetic forces at rotors' spin velocity 500 rad/sec	54
38 De-levitation with 20,000 lbs downward magnetic forces at spin velocity 500 rad/sec	54

LIST OF FIGURES (CONTINUED)

FIGURE		Page
39	Gimbal model.....	56
40	Ramp input simulation with gimbals at spin rate 500 rad/sec.....	56

LIST OF TABLES

TABLE	Page
1 Natural frequencies of vertical motion (Hz).....	13
2 Natural frequencies for θ motion at spin rate of 0 rad/sec (Hz).....	14
3 Natural frequencies for θ motion at spin rate of 500 rad/sec (Hz).....	14
4 Test data summary from Association of American Railroads (AAR)	24
5 Bump information	30
6 Parameters for catcher bearings	39
7 Maximum deflections and forces in the catcher bearings(AMB stiffness: 250,000 lbs/in; AMB damping ratio: 0.05; catcher bearing stiffness: 1,000,000 lbs/in; catcher bearing damping: 450 lb sec/in; rotors' spin rate:500rad/sec)	41
8 Main parameters for de-levitating model.....	48
9 Time to separate from catcher bearing for different AMB stiffness with gimbals	57
10 Time to separate from catcher bearing for different AMB stiffness without gimbals	57
11 Comparison of different methods for ramp support input.....	59

1. INTRODUCTION

1.1 Problem statement

Utilizing flywheels to store and reuse energy from regenerative braking on locomotives is a new technology being developed in the Vibration Control and Electromechanics Lab at Texas A&M. This technology promises to provide significant reductions in NOX emissions and diesel fuel consumption. The flywheels consist of a large inertia wheel weighing several tons and an integral motor/generator which is used to either increase the stored kinetic energy by motoring up the spin speed or converting the kinetic energy to electrical energy by operating the motor as a generator. The flywheel's spinning rotor is suspended on magnetic bearings which reduces parasitic drag losses. Backup bearings are installed to support the spinning rotor in the event of failure of the magnetic bearings. This thesis focuses on developing an approach to ensure the operating success of the magnetic and catcher bearings for a variety of support motion inputs which result from rail roughness, wheel out-of-roundness, bumps, etc.

1.2 Objective and significance

The objective is to determine if a passive isolation system can be designed to prevent collisions between the flywheel rotor and housing (stator) while the slug car supporting the flywheels experiences vertical and roll excitations, due to track / wheel profile irregularities and track elevation change inputs. The isolation system model is

This thesis follows the style of *Journal of Engineering Mechanics, ASCE*.

designed to protect the flywheel system from sinusoidal and ramp inputs. The sinusoidal input emulates the periodic profile variation, while the ramp input emulates the slug traversing a bump when entering or leaving a bridge.

Before the discussion of each input case, modeling of the system is required. There are three typical models: 1. Stack model (for sinusoidal input case), which uses floor motion as input and includes only flywheel stacks; 2. Whole model (for ramp input case), which includes car body, flywheel stacks, bogies and wheels. This model uses wheel and rail interaction as input; 3. Whole model with catcher bearings (for ramp input with de-levitation method), which adds catcher bearings to the original whole model but removes all the magnetic bearings.

To study the vibration isolation of the system, analytical and numerical integration (NI) methods are alternatively used. Analytical method, as the primary technique, helps the analysis in the frequency domain for sinusoidal input case. NI is used to simulate the ramp input case.

In this thesis, isolators J-6332-183 from Lord Company's FLEX-BOLT SANDWICH MOUNTS are chosen. Main parameters are as follows, maximum static load: 13,440 lbs; spring rate: 53,046 lb/in; damping ratio: $C/C_c=0.045$. The arrangement of isolators is shown in Fig. 1.

1.3 Literature review

Gangadharan, et al. 2008 applied finite element method to model the vehicle/track system and used Power Spectral Density (PSD) of track irregularities as input to the system. They directly applied the well-known PSD relations between inputs

and outputs. By doing so, they were able to generate PSD output profile. However, the response functions of the model (receptances) were not presented analytically. Furthermore, without the vertical velocity or acceleration PSD profile, the track vertical displacement PSD profile alone might not be enough for studying random vibration in a PSD manner.

There are also a limited number of track PSD or floor motion PSD profile resources. Ahmadian and Venezia 2000 carried out an experiment simulating the real train vibration under lab condition in order to get the PSD profile of floor vibration. They were able to build up the cab model and use a hydraulic oscillator as the input source. Association of American Railroads(Reiff and Robeda 2003) conducted a comprehensive test of the train vibration under operating conditions. The typical and worst-case data provided by them is widely used in this thesis.

For the modeling part, Thompson 1993 was among the earliest to model the wheel-rail interaction, but his focus was on the effect of track/soil vibration and noise propagation due to the interaction between wheel and rail. Park, et al. 2008 provided a 4-DOF prototype of flywheel system mounted on the train. However, their focus is also not on the vibration analysis.

There are also some vibration analysis based on random after the finding of well-known Wiener-Khinchine relations between the PSD and the autocorrelation function of a stationary random process. Singh and Chu 1976 used the SRSS (square-root-of-the-sum-of-the-squares) method in the earthquake engineering, in which they treated the problem with PSD input and PSD output. Singh 1980 derived the closed-form PSD

relations for non-proportional damping system. Through a 4 DOF non-proportional damping example, he showed that the RMS results by using exact and approximate methods (ignore all off-diagonal damping terms) are quite close. Ginsberg 2001 pointed out that for light damping case an approximate method can be used and the approximation may be expected to be quite good if all ξ_i values are found to be smaller than 0.1.

Subbiah, et al. 1985 studied the response of rotor system subjected to random excitations, which were assumed to be stationary and Gaussian with a white noise type of PSD. In this way, they found the peaks of PSD response corresponded to the natural frequencies. Boyce, et al. 1984 applied probabilistic method to design and analyze the foundation forces generated by unbalanced rotating machines. This paper showed the possibility of demonstrating the validity of PSD method by using numerical integration and probabilistic analysis. Kaul 1978 developed a method of generating spectrum-consistent time-history. This technique provides a conservative, while relatively accurate way to convert PSD profile from frequency domain to time domain.

2. MOTION ANALYSIS OF SINUSOIDAL INPUT

2.1 Introduction

If the track has a vertical perturbation due to periodic profile variation, large bounce and pitch oscillations of the vehicle can be generated(Shabana, et al. 2008). The bounce motion is defined as the vertical motion of the vehicle, while the pitch motion is defined as the rotation about an axis along the lateral direction of the vehicle. Because of the effect of gyroscopic, roll motion, which is defined as the rotation about an axis along the longitudinal direction of the car-body, can be generated along with the pitch motion. Our focus is the relative displacements between rotors and stators. And the design purpose is to ensure there is no collision between them.

Due to the availability of the floor acceleration in frequency domain provided by Ahmadian and Venezia 2000 and Association of American Railroads(AAR)(Reiff and Robeda 2003), sinusoidal floor input is used.

2.2 Model setup

There are five housings (layers) for one stack. Inside the housing, the rotor (flywheel) is supported by active magnetic bearings (AMBs) from x, y, and z direction. The isolators are mounted between layers in order to isolate vibration transmitted from the floor. Each layer is simplified into a plane with no thickness. Isolators and AMBs are modeled as springs and dampers as shown in Fig. 1. Though AMB is modeled as equivalent springs and dampers in this thesis, it is more complicated than spring and damper model in reality, i.e. it consists permanent magnet, electro-magnetic coils and a feedback controller. The stiffness of magnetic bearings, therefore, could be tuned by

changing the current in the electro-magnetic coils. For different distances away from magnetic bearings, the magnetic field is different, so is the magnetic force. Therefore, the stiffness of magnetic bearing is actually a parametric variable with respect to the gap between rotor and magnetic bearing. In this thesis, however, the magnetic bearing stiffness is assumed to be constant.

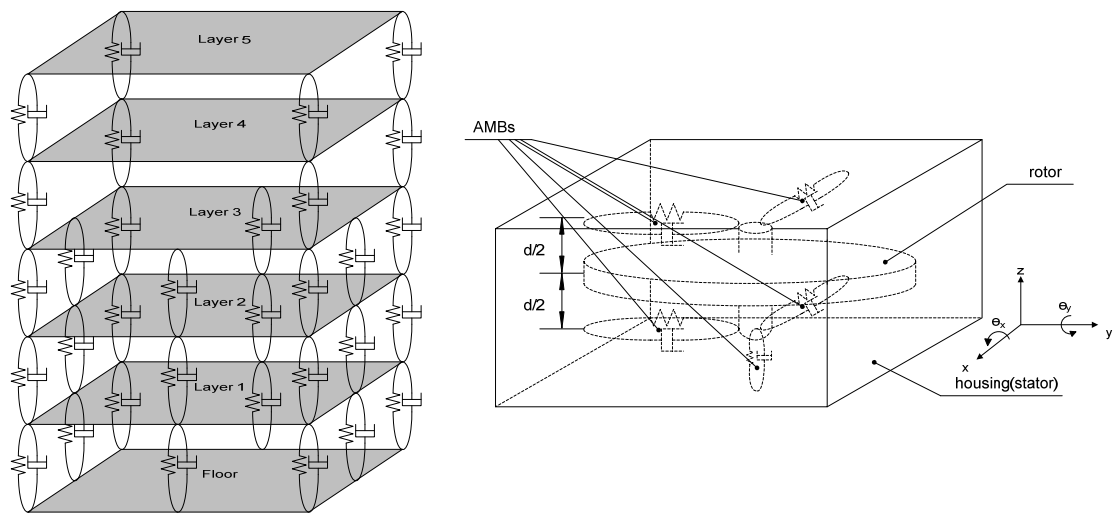
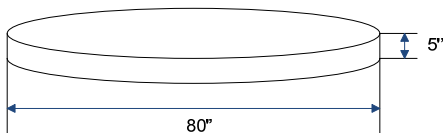


Fig. 1. Model setup

Model dimensions are shown in Fig. 2 with specific parameters listed below.

Rotor:



Stator:

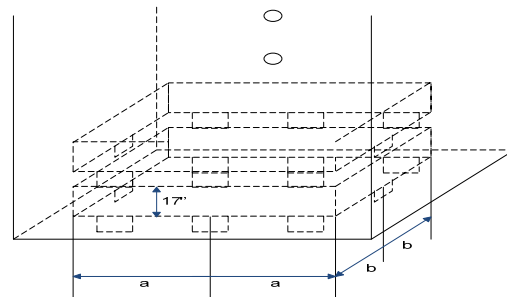


Fig. 2. Model dimensions

- Housing:

Mass: $m_1 = m_2 = m_3 = m_4 = m_5 = 4000 / 386 \text{ lbs s}^2/\text{in}$;

Mass moment of inertia

About x axis: $I_{x1} = I_{x2} = I_{x3} = I_{x4} = I_{x5} = 4250 \text{ lbs} \cdot \text{s}^2 \cdot \text{in}$;

About y axis: $I_{y1} = I_{y2} = I_{y3} = I_{y4} = I_{y5} = 4250 \text{ lbs} \cdot \text{s}^2 \cdot \text{in}$;

Geometric dimension: a = 45'', b = 45'';

- Rotor:

Mass of rotor: $m_{r1} = m_{r2} = m_{r3} = m_{r4} = m_{r5} = 8000 / 386 \text{ lbs s}^2/\text{in}$;

Mass moment of inertia

About x axis: $I_{rx1} = I_{rx2} = I_{rx3} = I_{rx4} = I_{rx5} = I_T = 8500 \text{ lbs} \cdot \text{s}^2 \cdot \text{in}$;

About y axis: $I_{ry1} = I_{ry2} = I_{ry3} = I_{ry4} = I_{ry5} = I_T = 8500 \text{ lbs} \cdot \text{s}^2 \cdot \text{in}$;

About z axis: $I_p = 17000 \text{ lbs} \cdot \text{s}^2 \cdot \text{in}$;

Geometric dimensions:

Diameter: 80'', thickness: 5'';

- Isolators:

Stiffness for each one: $k = 53046 \text{ lbs} / \text{in}$;

Damping ratio: $\xi = 0.045$;

Damping for layer 1(each isolator):

$$c_1 = 2 \cdot M \cdot \omega_n \cdot \xi \approx 2\xi \sqrt{k \cdot M} = 2 * 0.045 * \sqrt{53046 * (60000 / 386 / 8)} = 91.4 \text{ lbs} \cdot \text{sec} / \text{in} ;$$

Damping for layer 2(each isolator): $c_2 = 81.7 \text{ lbs} \cdot \text{sec} / \text{in}$;

Damping for layer 3(each isolator): $c_3 = 70.8 \text{ lbs} \cdot \text{sec} / \text{in}$;

Damping for layer 4(each isolator): $c_4 = 66.7 \text{ lbs} \cdot \text{sec} / \text{in}$;

Damping for layer 5(each isolator): $c_5 = 47.2 \text{ lbs} \cdot \text{sec} / \text{in}$;

- Active Magnetic Bearings (AMBs):

Stiffness for x, y, z direction: $k_x = k_y = k_z = 1,000 \text{ lbs} / \text{in}$;

Damping ratio: $\xi_1 = 0.05$;

$$\text{Damping: } c_x = c_y = \frac{4 \cdot I_T \cdot \xi_1}{d^2} \sqrt{\frac{k_x \cdot d^2}{2 \cdot I_T}} = 82.46 \text{ lbs} \cdot \text{sec} / \text{in} ,$$

$$c_z = 2 \cdot \xi_1 \cdot \sqrt{k_z \cdot m_r} = 14.4 \text{ lbs} \cdot \text{sec} / \text{in} ;$$

2.3 Force analysis

For the sake of illustration, only the first layer is analyzed in detail.

2.3.1 For rotor

Consider bounce, pitch and roll motion only, and suppose $Z_{r1} > Z_1$, $\theta_{rx1} > \theta_{x1}$, $\theta_{ry1} > \theta_{y1}$ (assume small motion $\sin \theta \approx \theta$). Fig. 3 illustrates stack layout. The free body diagram (FBD) of the interaction between rotor and housing is shown in Fig. 4.

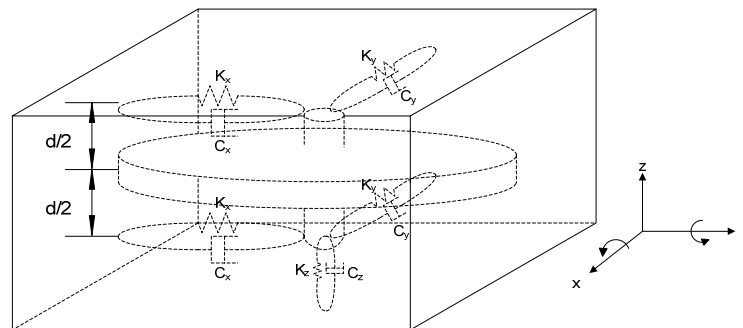


Fig. 3. Stack layout

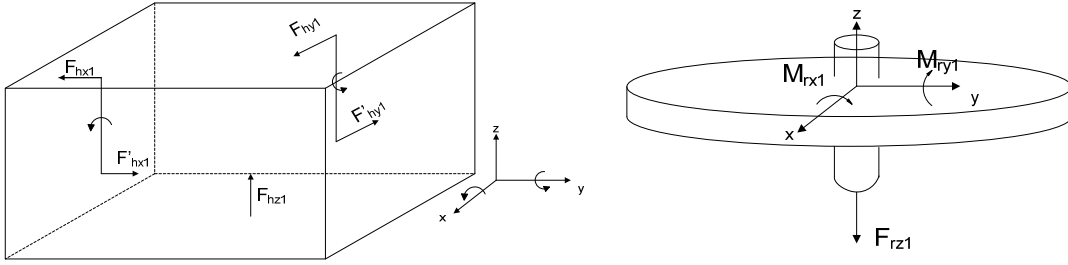


Fig. 4. FBD of housing and rotor

Because of the geometric symmetry, $F_{hx1} = F'_{hx1}$, $F_{hy1} = F'_{hy1}$, forces in x, y directions are balanced.

2.3.1.1 θ_x -motion analysis (θ_y -motion is identical to θ_x -motion)

Horizontal displacement due to the difference between rotor's and housing's θ_x -motion:

$$\delta_{rx1} = (\theta_{rx1} - \theta_{x1}) \cdot \frac{d}{2} \quad (2.1)$$

Horizontal force on housing_1:

$$F_{hx1} = \delta_{rx1} \cdot k_x + \dot{\delta}_{rx1} \cdot c_x \quad (2.2)$$

According to Newton's third law, force on rotor_1 is:

$$F_{rx1} = -F_{hx1} \quad (2.3)$$

Moment on housing_1 in θ_x direction is:

$$\begin{aligned} M_{hx1} &= F_{rx1} \cdot \frac{d}{2} + F_{rx1} \cdot \frac{d}{2} \\ &= F_{rx1} \cdot d \\ &= k_r \cdot \theta_{rx1} \cdot \frac{d^2}{2} + c_r \cdot \dot{\theta}_{rx1} \cdot \frac{d^2}{2} - k_r \cdot \theta_{x1} \cdot \frac{d^2}{2} - c_r \cdot \dot{\theta}_{x1} \cdot \frac{d^2}{2} \end{aligned} \quad (2.4)$$

Therefore, moment on the rotor_1 is:

$$M_{rx1} = -M_{hx1} \quad (2.5)$$

From Vance(Vance 1988), Equations of motion(EOMs) for rotor are in the form of:

$$\begin{aligned} I_x \cdot \ddot{\theta}_{rx} + (I_p \omega) \cdot \dot{\theta}_{ry} &= \sum M_{rx} \\ I_y \cdot \ddot{\theta}_{ry} - (I_p \omega) \cdot \dot{\theta}_{rx} &= \sum M_{ry} \end{aligned} \quad (2.6)$$

In which, $+(I_p \omega) \cdot \dot{\theta}_{ry}$ and $-(I_p \omega) \cdot \dot{\theta}_{rx}$ terms are due to gyroscopic effect. (ω is the spin velocity of rotor)

2.3.1.2 z-motion analysis

Vertical force on housing_1 due to the rotor:

$$F_{hz1} = (z_{r1} - z_1) \cdot k_r + (\dot{z}_{r1} - \dot{z}_1) \cdot c_r \quad (2.7)$$

Therefore, vertical force on rotor_1 is:

$$F_{rz1} = -F_{hz1} \quad (2.8)$$

From Newton's law and (2.6), EOMs for rotor_1 are:

$$m_{r1} \cdot \ddot{Z}_{r1} = F_{rz1} \quad (2.9)$$

$$I_{rx1} \cdot \ddot{\theta}_{rx1} + (I_p \omega) \cdot \dot{\theta}_{ry1} = M_{rx1} \quad (2.10)$$

$$I_{ry1} \cdot \ddot{\theta}_{ry1} - (I_p \omega) \cdot \dot{\theta}_{rx1} = M_{ry1} \quad (2.11)$$

2.3.2 For housing

Again, only consider bounce, pitch and roll motion, and suppose $Z_2 > Z_1 > Z_0$,

$\theta_{x2} > \theta_{x1} > \theta_{x0}$, $\theta_{y2} > \theta_{y1} > \theta_{y0}$. Fig. 5 shows the FBD of the first layer.

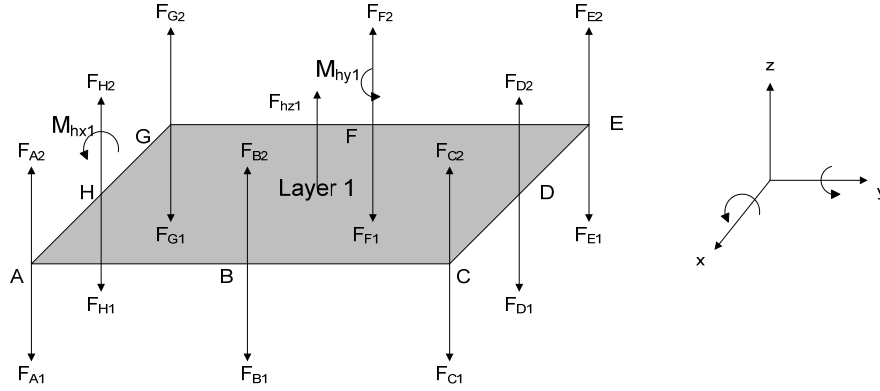


Fig. 5. FBD for housing_1

From Newton's law:

$$m_1 \cdot \ddot{Z}_1 = (F_{A2} + F_{B2} + \dots + F_{H2}) - (F_{A1} + F_{B1} + \dots + F_{H1}) + F_{hz1} \quad (2.12)$$

$$I_{x1} \cdot \ddot{\theta}_{x1} = (F_{C2} - F_{C1} + F_{D2} - F_{D1} + F_{E2} - F_{E1}) \cdot a - (F_{A2} - F_{A1} + F_{G2} - F_{G1} + F_{H2} - F_{H1}) \cdot a + M_{hx1} \quad (2.13)$$

$$I_{y1} \cdot \ddot{\theta}_{y1} = (F_{E2} - F_{E1} + F_{F2} - F_{F1} + F_{G2} - F_{G1}) \cdot b - (F_{A2} - F_{A1} + F_{B2} - F_{B1} + F_{C2} - F_{C1}) \cdot b + M_{hy1} \quad (2.14)$$

In which, $M_{hx1} = -M_{rx1}$, $M_{hy1} = -M_{ry1}$, according to (2.5).

Combine all the EOMs to form:

$$\begin{aligned}
& \begin{pmatrix} \ddot{Z}_1 \\ \ddot{Z}_{r1} \\ \vdots \\ \ddot{Z}_5 \\ \ddot{Z}_{r5} \\ \ddot{\theta}_{x1} \\ \ddot{\theta}_{y1} \\ \ddot{\theta}_{rx1} \\ \ddot{\theta}_{ry1} \\ \vdots \\ \ddot{\theta}_{x5} \\ \ddot{\theta}_{y5} \\ \ddot{\theta}_{rx5} \\ \ddot{\theta}_{ry5} \end{pmatrix}_{30 \times 1} \cdot \underline{\underline{M}}_{30 \times 30} + \begin{pmatrix} \dot{Z}_1 \\ \dot{Z}_{r1} \\ \vdots \\ \dot{Z}_5 \\ \dot{Z}_{r5} \\ \dot{\theta}_{x1} \\ \dot{\theta}_{y1} \\ \dot{\theta}_{rx1} \\ \dot{\theta}_{ry1} \\ \vdots \\ \dot{\theta}_{x5} \\ \dot{\theta}_{y5} \\ \dot{\theta}_{rx5} \\ \dot{\theta}_{ry5} \end{pmatrix}_{30 \times 1} \cdot \underline{\underline{C}}_{30 \times 30} + \begin{pmatrix} Z_1 \\ Z_{r1} \\ \vdots \\ Z_5 \\ Z_{r5} \\ \theta_{x1} \\ \theta_{y1} \\ \theta_{rx1} \\ \theta_{ry1} \\ \vdots \\ \theta_{x5} \\ \theta_{y5} \\ \theta_{rx5} \\ \theta_{ry5} \end{pmatrix}_{30 \times 1} \cdot \underline{\underline{K}}_{30 \times 30} = \begin{pmatrix} 8 \cdot k_1 \cdot Z_f(t) + 8 \cdot c_1 \cdot \dot{Z}_f(t) \\ 0 \\ \vdots \\ 0 \\ 0 \\ 6 \cdot k_1 \cdot a^2 \cdot \theta_{yf}(t) + 6 \cdot c_1 \cdot a^2 \cdot \dot{\theta}_{yf}(t) \\ 6 \cdot k_1 \cdot b^2 \cdot \theta_{yf}(t) + 6 \cdot c_1 \cdot b^2 \cdot \dot{\theta}_{yf}(t) \\ 0 \\ 0 \\ \vdots \\ 0 \\ 0 \\ 0 \\ 0 \\ 0 \end{pmatrix}_{30 \times 1} \quad (2.15)
\end{aligned}$$

$\underline{\underline{M}}$, $\underline{\underline{C}}$, $\underline{\underline{K}}$ are given in Appendix A. Z_f and θ_f are floor motions in Z and θ directions. Since Z and θ_x , θ_y motion are de-coupled, it is possible to analyze z motion and θ motion separately.

2.4 System properties

2.4.1 Natural frequencies for z motion

The general form of EOM is:

$$\underline{\underline{M}} \cdot \ddot{\underline{q}} + \underline{\underline{C}} \cdot \dot{\underline{q}} + \underline{\underline{K}} \cdot \underline{q} = 0 \quad (2.16)$$

If $\underline{V} = \begin{Bmatrix} \underline{q} \\ \dot{\underline{q}} \end{Bmatrix}$, $\dot{\underline{V}} = \begin{Bmatrix} \dot{\underline{q}} \\ \ddot{\underline{q}} \end{Bmatrix}$, then (2.16) can be written as

$$\dot{\underline{V}} = \begin{pmatrix} \underline{0} & \underline{I} \\ -\underline{\underline{M}}^{-1} \underline{\underline{K}} & -\underline{\underline{M}}^{-1} \underline{\underline{C}} \end{pmatrix} \cdot \underline{V} \quad (2.17)$$

$\begin{pmatrix} \underline{0} & \underline{I} \\ -\underline{M}^{-1}\underline{K} & -\underline{M}^{-1}\underline{C} \end{pmatrix}$ is the characteristic matrix and $\lambda_i \left\{ \begin{pmatrix} \underline{0} & \underline{I} \\ -\underline{M}^{-1}\underline{K} & -\underline{M}^{-1}\underline{C} \end{pmatrix} \right\}$ are

the natural frequencies of the system. Table 1 lists undamped natural frequencies for vertical motion.

Table 1. Natural frequencies of vertical motion (Hz)

1.0862	1.1013	1.1031	1.1035	1.1038
8.6946	21.564	35.351	43.645	56.496

2.4.2 Natural frequencies for θ_x , θ_y motion

Since the C matrix in (2.15) contains gyroscopic term $I_p\omega$ (ω is the spin velocity of the rotor), natural frequencies for θ_x , θ_y would vary with different ω . Using the same method as used for solving natural frequencies of Z-motion, their relations are plotted in Fig. 6. In the magnified picture, the increasing curve represents forward whirling motion, while the decreasing one represents backward whirling motion.

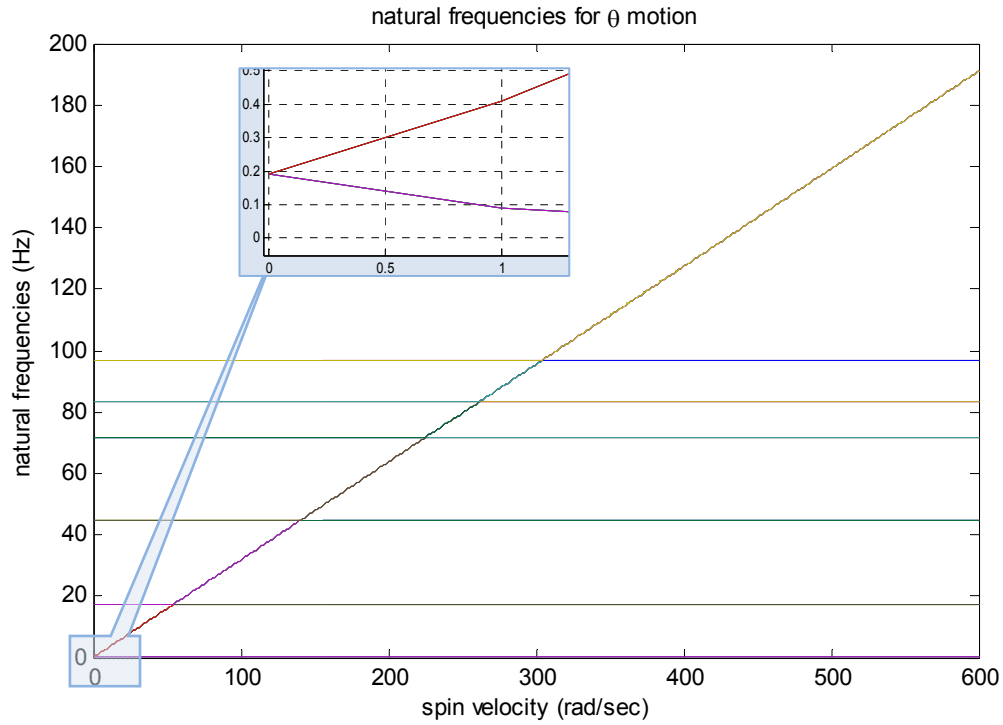


Fig. 6. θ -motion natural frequencies vary with spin velocity

At spin velocity $\Omega=0$ rad/sec, θ motion natural frequencies are listed in Table 2.

Table 2. Natural frequencies for θ motion at spin rate of 0 rad/sec (Hz)

0.19	0.19	0.19	0.19	0.19	0.19	0.19	0.19	0.19	0.19
17.00	17.00	44.65	44.65	71.45	71.45	83.23	83.23	96.55	96.55

At spin velocity $\Omega=500$ rad/sec, θ motion natural frequencies are listed in Table 3.

Table 3. Natural frequencies for θ motion at spin rate of 500 rad/sec (Hz)

0.00	0.00	0.00	0.00	0.00	17.00	17.00	44.65	44.65	71.45
71.45	83.23	83.23	96.55	96.55	159.16	159.16	159.16	159.16	159.16

2.4.3 Transmissibility

Given the EOMs in matrix form (2.15).

For z motion

Suppose: $Z_f = A \cdot e^{i\omega t}$, $\dot{Z}_f = A \cdot \omega \cdot e^{i\omega t} \cdot i$, $\ddot{Z}_f = -A \cdot \omega^2 \cdot e^{i\omega t}$

$$Z_1 = A_1 \cdot e^{i\omega t}, \dot{Z}_1 = A_1 \cdot \omega \cdot e^{i\omega t} \cdot i, \ddot{Z}_1 = -A_1 \cdot \omega^2 \cdot e^{i\omega t} \text{ and so on.}$$

Then, $e^{i\omega t}$ term can be cancelled, leaving magnitude and frequency as unknown.

$$-\underline{M} \cdot \underline{A}_{10 \times 1} \cdot \omega^2 + \underline{C} \cdot \underline{A}_{10 \times 1} \cdot \omega \cdot i + \underline{K} \cdot \underline{A}_{10 \times 1} = \begin{pmatrix} 8 \cdot k_1 \cdot A + 8 \cdot c_1 \cdot A \cdot \omega \cdot i \\ 0 \\ \vdots \\ 0 \\ 0 \end{pmatrix}_{10 \times 1} \quad (2.18)$$

$$\text{Where } \underline{A}_{10 \times 1} = [A_1 \ A_{r1} \ A_2 \ A_{r2} \ \cdots \ A_5 \ A_{r5}]^T.$$

We can also write EOMs in the relative form (2.19). Replace $[Z_1 \ Z_{r1} \ \cdots \ Z_5]^T$ with

$[Z_{R_1} + Z_f \ Z_{R_{r1}} + Z_f \ \cdots \ Z_{R_5} + Z_f]^T$, where $[Z_1 \ Z_{r1} \ \cdots \ Z_5]^T$ represents absolute motion,

while $[Z_{R_1} \ Z_{R_{r1}} \ \cdots \ Z_{R_5}]^T$ represents relative motion with respect to floor motion,

which is denoted as Z_f .

$$\underline{M} \cdot \ddot{\underline{Z}}_{R_{10 \times 1}} + \underline{C} \cdot \dot{\underline{Z}}_{R_{10 \times 1}} + \underline{K} \cdot \underline{Z}_{R_{10 \times 1}} = \begin{pmatrix} -m_1 \cdot \ddot{Z}_f \\ -m_{r1} \cdot \ddot{Z}_f \\ \vdots \\ -m_5 \cdot \ddot{Z}_f \\ -m_{r5} \cdot \ddot{Z}_f \end{pmatrix}_{10 \times 1} \quad (2.19)$$

in which, $\ddot{\underline{Z}}_f = -A \cdot \omega^2 \cdot e^{i\omega t}$;

$$\underline{\dot{Z}}_R = \underline{A}_R \cdot e^{i\omega t}, \underline{\dot{Z}}_R = \underline{A}_R \cdot \omega \cdot e^{i\omega t} \cdot i, \underline{\ddot{Z}}_R = -\underline{A}_R \cdot \omega^2 \cdot e^{i\omega t} ;$$

Therefore, (2.19) can be further written into,

$$-\underline{M} \cdot \underline{A}_{R_{10 \times 1}} \cdot \omega^2 + \underline{C} \cdot \underline{A}_{R_{10 \times 1}} \cdot \omega \cdot i + \underline{K} \cdot \underline{A}_{R_{10 \times 1}} = \begin{pmatrix} m_1 \cdot A \cdot \omega^2 \\ m_{r1} \cdot A \cdot \omega^2 \\ \vdots \\ m_5 \cdot A \cdot \omega^2 \\ m_{r5} \cdot A \cdot \omega^2 \end{pmatrix}_{10 \times 1} \quad (2.20)$$

The basic \underline{M} , \underline{C} , \underline{K} matrices remained the same as those in (2.18). Only external force terms changed from complex expressions to real expressions, which make manipulation much easier. Another advantage of (2.20) is that, it allows us to directly make use of floor acceleration which is usually measured by accelerometer. By applying the relative form, we spared the anxiety of figuring out the amplitude of displacement and velocity, and the phase difference between them.

Solve \underline{A}_R from (2.20),

$$\underline{A}_{R_{10 \times 1}} = \text{inv}(-\underline{M} \cdot \omega^2 + i \cdot \omega \cdot \underline{C} + \underline{K}) \cdot A \omega^2 \cdot \begin{pmatrix} m_1 \\ m_{r1} \\ \vdots \\ m_5 \\ m_{r5} \end{pmatrix}_{10 \times 1} \quad (2.21)$$

Divide A on both sides,

$$\begin{pmatrix} A_{R1} / A \\ A_{Rr1} / A \\ \vdots \\ A_{R5} / A \\ A_{Rr5} / A \end{pmatrix}_{10 \times 1} = \text{inv}(-\underline{M} \cdot \omega^2 + i \cdot \omega \cdot \underline{C} + \underline{K}) \cdot \omega^2 \cdot \begin{pmatrix} m_1 \\ m_{r1} \\ \vdots \\ m_5 \\ m_{r5} \end{pmatrix}_{10 \times 1} \quad (2.22)$$

A_R / A is defined as transmissibility in the z direction. The transmissibility vs. excitation frequencies is shown in Fig. 7.

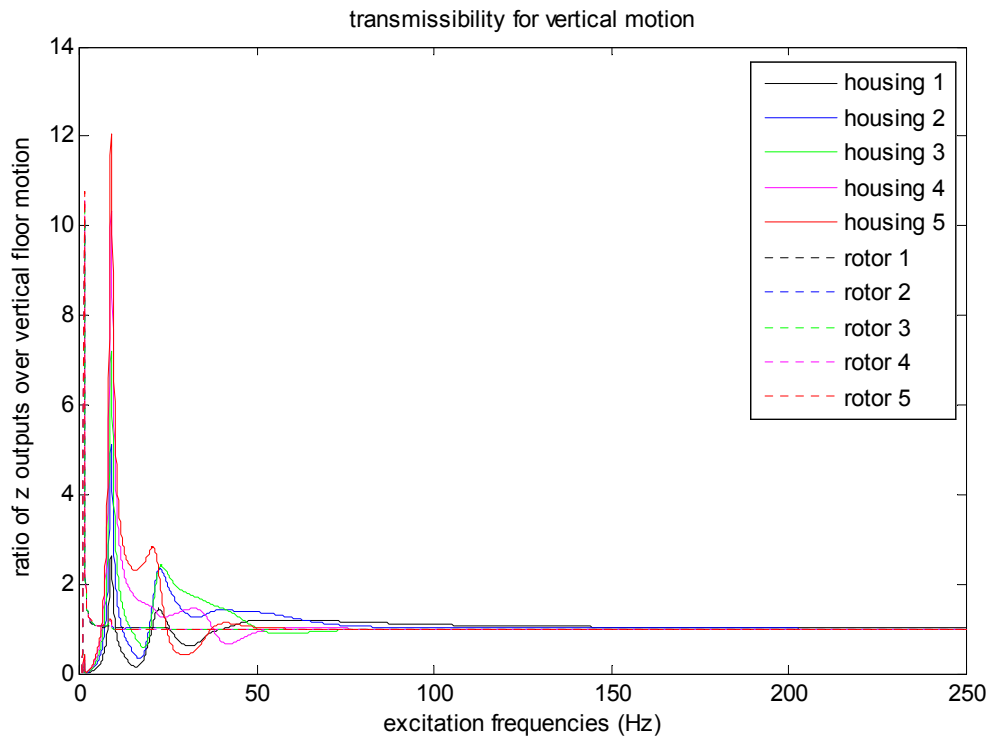


Fig. 7. Transmissibility of z motion

From above graph, we can see that the resonant peak for housing motion happens at about 8.7 Hz, while for rotor motion, resonance happens around 1 Hz.

For θ motion

$$\text{Suppose: } \theta_{xf} = B \cdot e^{i\omega t}, \dot{\theta}_{xf} = B \cdot \omega \cdot e^{i\omega t} \cdot i, \ddot{\theta}_{xf} = -B \cdot \omega^2 \cdot e^{i\omega t}$$

$$\theta_{yf} = 0 \text{ (only } \theta_x \text{ input)}$$

$$\theta_{x1} = B_{x1} \cdot e^{i\omega t}, \dot{\theta}_{x1} = B_{x1} \cdot \omega \cdot e^{i\omega t} \cdot i, \ddot{\theta}_{x1} = -B_{x1} \cdot \omega^2 \cdot e^{i\omega t}$$

$$\theta_{y1} = B_{y1} \cdot e^{i\omega t}, \dot{\theta}_{y1} = B_{y1} \cdot \omega \cdot e^{i\omega t} \cdot i, \ddot{\theta}_{y1} = -B_{y1} \cdot \omega^2 \cdot e^{i\omega t} \text{ and so on.}$$

Then, through the similar manipulation as z motion, we get transmissibility of θ motion.

$$\begin{pmatrix} B_{Rx1} / B \\ B_{Ry1} / B \\ B_{Rrx1} / B \\ B_{Rry1} / B \\ \vdots \end{pmatrix}_{20 \times 1} = \text{inv}(-\underline{M} \cdot \omega^2 + i \cdot \omega \cdot \underline{C}(\Omega) + \underline{K}) \cdot \omega^2 \cdot \begin{pmatrix} I_{x1} \\ I_{y1} \\ I_{rx1} \\ I_{ry1} \\ \vdots \end{pmatrix}_{20 \times 1} \quad (2.23)$$

in which B_R denotes relative amplitude with respect to floor.

Because $C(\Omega)$ changes with spin velocity Ω , the transmissibility also depends on spin velocity Ω . At spin velocity $\Omega=500$ rad/sec, which is the operation speed, the transmissibility vs. excitation frequencies is shown in Fig. 8.

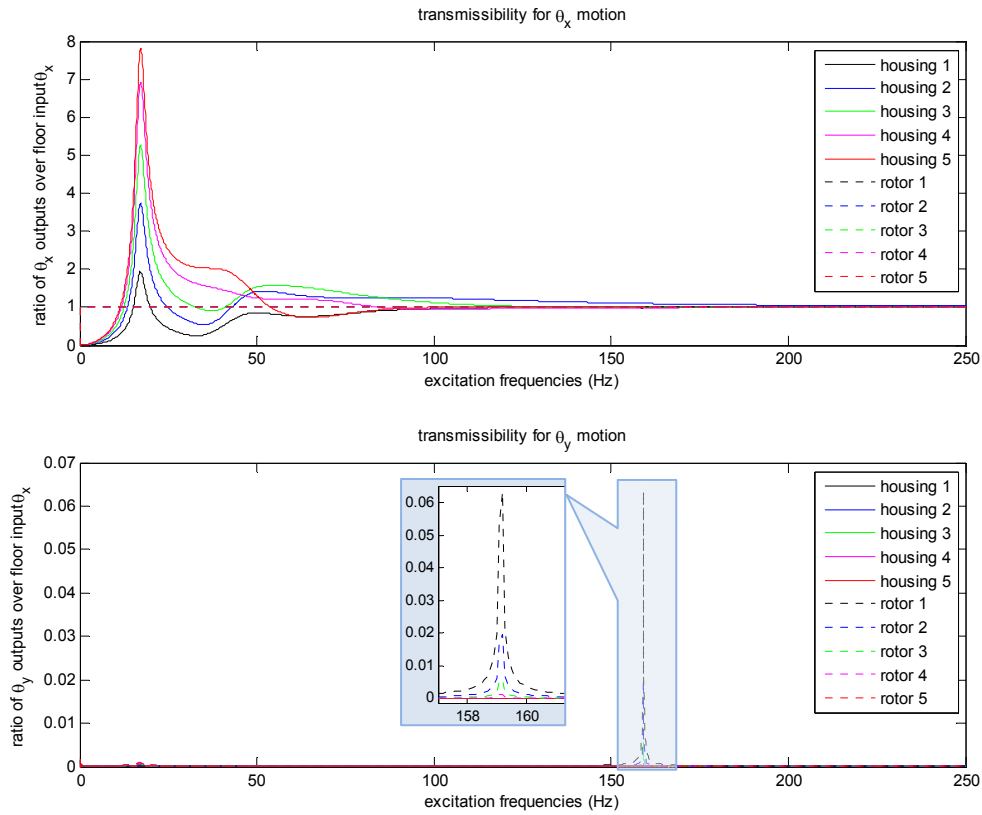


Fig. 8. Transmissibility of θ motion

From upper graph in Fig. 8, we can see that the resonant peak for the housing motion happens around 20 Hz. Rotors are insensitive to the input because their transmissibilities are always 1, which means rotors almost stand still given whatever input frequency. From bottom graph in Fig. 8, we see that even though θ_x and θ_y motions are coupled, given only θ_x motion will not affect θ_y much. Therefore, the effect of θ_y motion can be neglected in the later discussion of the relative motion calculation.

2.4.4 Relative motion of rotors with respect to housings

1st layer's relative motion in the z direction can be written as:

$$\Delta Z_1 = [-1 \ 1 \ 0 \ \dots \ 0]_{1 \times 10} \cdot \begin{bmatrix} Z_{R1} \\ Z_{Rr1} \\ \vdots \\ Z_{R5} \\ Z_{Rr5} \end{bmatrix}_{10 \times 1} \quad (2.24)$$

1st layer's relative motion in the θ direction can be written as: (as discussed earlier, θ_y motion is neglected intentionally)

$$\Delta \theta_{x1} = [-1 \ 0 \ 1 \ 0 \ \dots \ 0]_{1 \times 20} \cdot \begin{bmatrix} \theta_{Rx1} \\ \theta_{Ry1} \\ \theta_{Rrx1} \\ \theta_{Rry1} \\ \vdots \end{bmatrix}_{20 \times 1} \quad (2.25)$$

Other layers can be written in the similar form.

Therefore, the largest relative motion (refer to the Fig. 9) of layer 1 is:

$$\Delta l = abs(A \cdot [-1 \ 1 \ 0 \ \dots \ 0]_{1 \times 10} \cdot \begin{bmatrix} Z_{R1} \\ Z_{Rr1} \\ \vdots \\ Z_{R5} \\ Z_{Rr5} \end{bmatrix}_{10 \times 1}) + abs(aa \cdot B \cdot [-1 \ 0 \ 1 \ 0 \ \dots \ 0]_{1 \times 20} \cdot \begin{bmatrix} \theta_{Rx1} \\ \theta_{Ry1} \\ \theta_{Rrx1} \\ \theta_{Rry1} \\ \vdots \end{bmatrix}_{20 \times 1}) \quad (2.26)$$

Where, A is the amplitude of Z motion input;

B is the amplitude of θ_x motion input;

aa is the radius of the rotor.

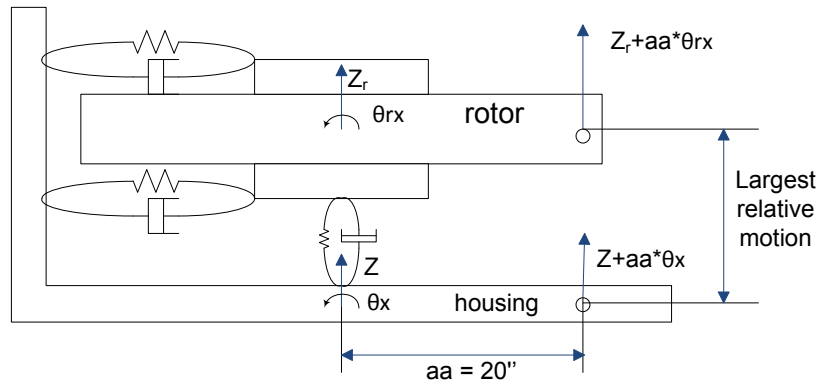


Fig. 9. Definition of largest relative motion

In the same way, $\Delta_2, \dots, \Delta_5$, which represent the largest relative motion of layer2, ..., layer5, can be written in the similar form.

2.5 Source of input

Source 1: experimental data from Ahmadian and Venezia 2000, where floor acceleration data in locomotive cab was collected. A setup of locomotive cab was built in order to: 1. Establish the vibration characteristics of a typical cab used in freight locomotives in North America, and 2. Evaluate the effect of various structural modifications on the interior cab noise. The cab model was placed on four Goodyear air springs and was excited by a hydraulic actuation system consisting of a hydraulic pump, manifold, and actuator.

Floor acceleration profiles at center, lateral side, and longitudinal side are used in this thesis for sinusoidal input simulation.

For pure vertical floor vibration, data at location 6 is used. And $\frac{|Z_1|+|Z_6|}{a}$ (a is assumed to be the length of cab) is used as θ_x input, $\frac{|Z_7|+|Z_6|}{b}$ (b is assumed to be the

width of cab) as θ_y input. Since there is no phase information for θ_x , and θ_y floor input, we only set one input at one time, i.e., if $\theta_{xf} = B \cdot \sin(\omega t)$, then $\theta_{yf} = 0$. And because θ motions are coupled with rotors' spin velocity, in order to simulate the worst case, the frequency at which peak input displacement happens is used to calculate rotors' spin velocity so that the natural frequencies would be excited by the frequency that peak input displacement occurs.

From Fig. 10, θ_x 's peak input happens at about 10 Hz. And from the spin speed and natural frequencies relation in Fig. 6, when rotors are running at about 35 rad/sec, natural frequency of rotors would be at 10 Hz. This is the worst scenario, which will be verified by simulation over all spin speeds later.

Reproduced input sinusoidal signals (z , θ_x) in frequency domain from Ahmadian and Venezia 2000 are shown in Fig. 10.

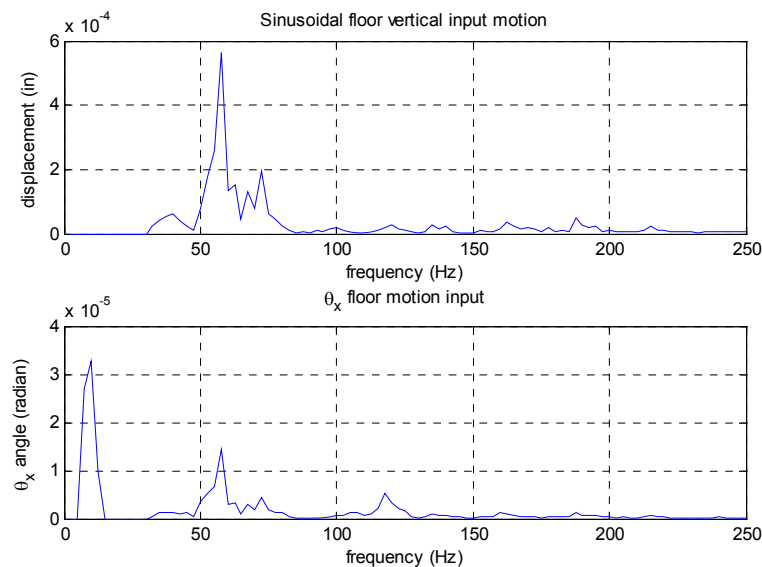


Fig. 10. Sinusoidal input signals (z , θ_x)

Source 2: field data from AAR report(Reiff and Robeda 2003).

The vibration tests were conducted by Transportation Technology Center, Inc. (TTCI), a subsidiary of the Association of American Railroads (AAR). Two field data were collected (auto parts and coal). The tests were based on 660-mile route, 21 hours with average speed 60-70 MPH test and 480-mile route, 28 hours test. The data it collected represents the worst-case vibration scenario.

Data Analysis:

Time domain statistics

Over 20 hours of vibration measurements were recorded for each field test, automatically segmented into file lengths of 5 to 6 minutes each. These files were sorted to yield those containing the largest vibration root-mean-square (RMS) values and largest peak values. Specifications: 2000 samples per second, anti-alias filters set to 1 KHz.

Frequency domain transformations

Specifications: spectral resolution 2 Hz; Amplitude units g^2/Hz

Test data summary at cab location in vertical direction is shown in Table 4.

(Using 20 breakpoints)

Table 4. Test data summary from Association of American Railroads (AAR)(Reiff and Robeda 2003)

Break Frequency (Hz)	Field Extremes (g*g/Hz)	Equivalent displacement (in)
2	8.09e-4	0.09832
10	1.35e-3	0.00508
20	1.35e-2	0.00402
34	2.32e-2	0.00182
60*	2.78e-1*	0.00203*
80	5.80e-3	0.00016
146	2.32e-2	0.00010
170	2.02e-3	0.00002
190	1.39e-2	0.00005
220	9.17e-4	0.00001
230	8.12e-3	0.00002
270	9.28e-3	0.00002
290	2.32e-3	0.00001
332	9.25e-1	0.00012
420	2.43e-4	0.00000
440	4.64e-3	0.00000
480	1.62e-4	0.00000
700	1.16e-3	0.00000
870	3.51e-4	0.00000
1024	2.32e-3	0.00000

(* represents the extreme data)

Compare the data with previous source, we found AAR data is more conservative. Peak value is more than 3 times than peak value reproduced from Ahmadian and Venezia 2000, whereas the corresponding frequencies are the same, at 60 Hz.

2.6 Simulation results

By applying the input data (only consider z and θ_x input) and largest relative motion expression (2.26), relative motion between rotor and housing varying with frequencies is shown in Fig. 11 using operation spin velocity $\Omega = 500$ rad/sec.

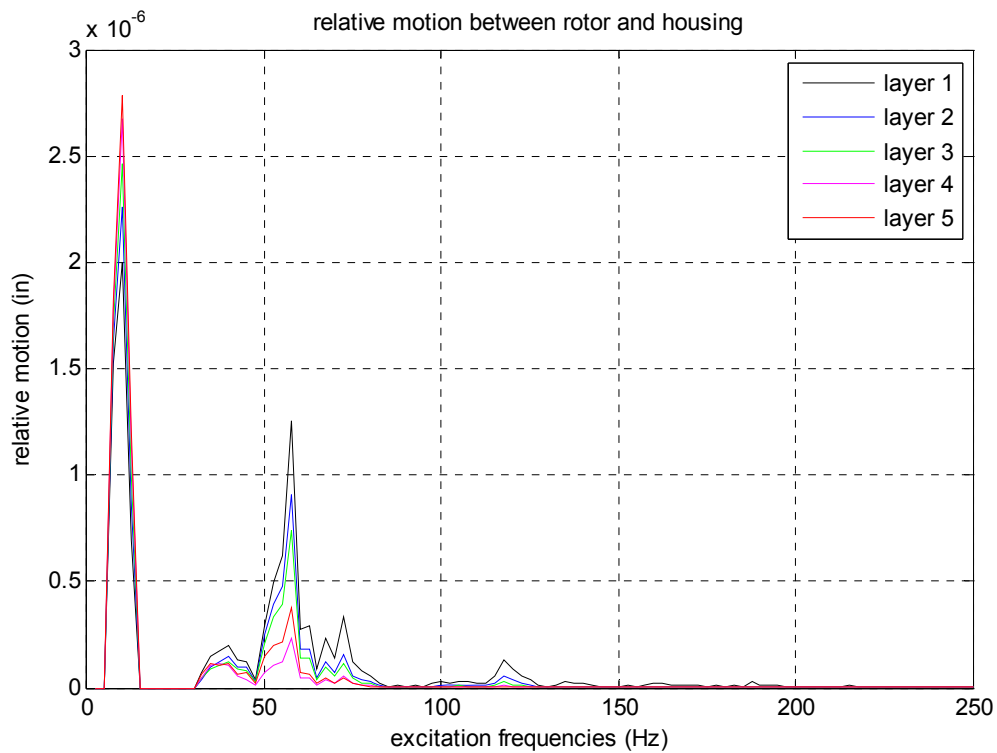


Fig. 11. Relative motion between rotor and housing due to sinusoidal floor input

As can be seen, the largest relative motion is 2.8×10^{-6} inch at excitation frequency 10 Hz, while our gap requirement between rotor and housing is less than 0.02 inch. Therefore, it is quite acceptable.

Since the largest relative vibration does not necessarily happen at spin velocity $\Omega=500$ rad/sec, we need to search for all spin velocity and all excitation frequencies in

order to find the largest relative motion. By varying spin velocity from 0 to 500 rad/sec, the largest relative motion varies in a small scale, from 1.9736×10^{-6} inch to 2.0131×10^{-6} inch. It is found that, at spin velocity 31 rad/sec maximum relative motion 2.0131×10^{-6} inch happens. This verifies the prediction that maximum relative motion occurs at spin speed about 35 rad/sec.

Using AAR's data throughout 2~250 Hz range as vertical input, Fig. 12 shows the largest relative motion outputs at AMB stiffness 1,000 lbs/in, Fig. 13 shows outputs at AMB stiffness of 250,000 lbs/in. As can be seen, at low AMB stiffness, maximum relative motion happens to be 0.013 inch at 2 Hz. However, at 250,000 lbs/in AMB stiffness, the relative motion can be limited within a small value. In this case, the maximum relative displacement is about 6×10^{-5} inch at 6 Hz.

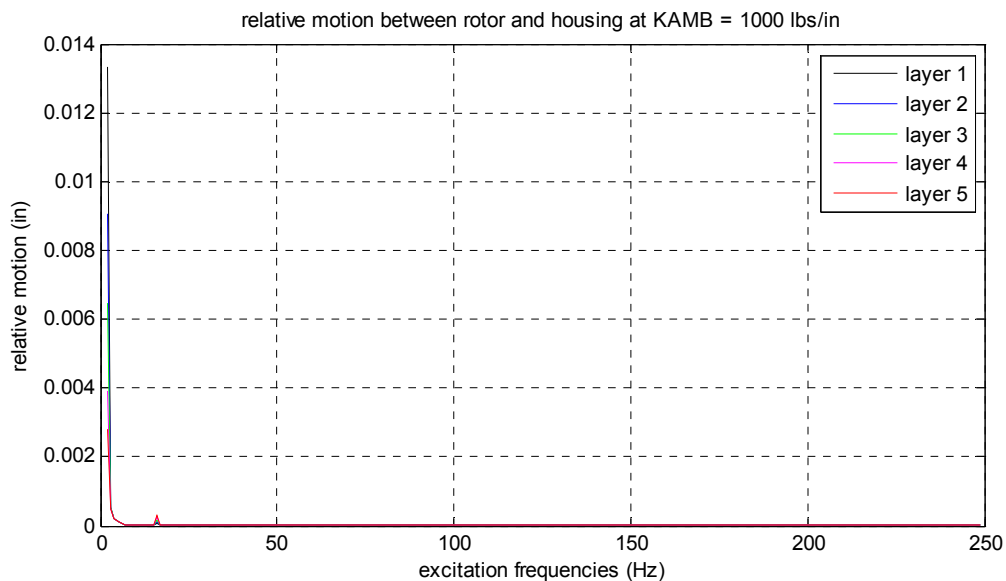


Fig. 12. Relative motion due to sinusoidal floor input in vertical direction from AAR's data at $K_{AMB} = 1000$ lbs/in

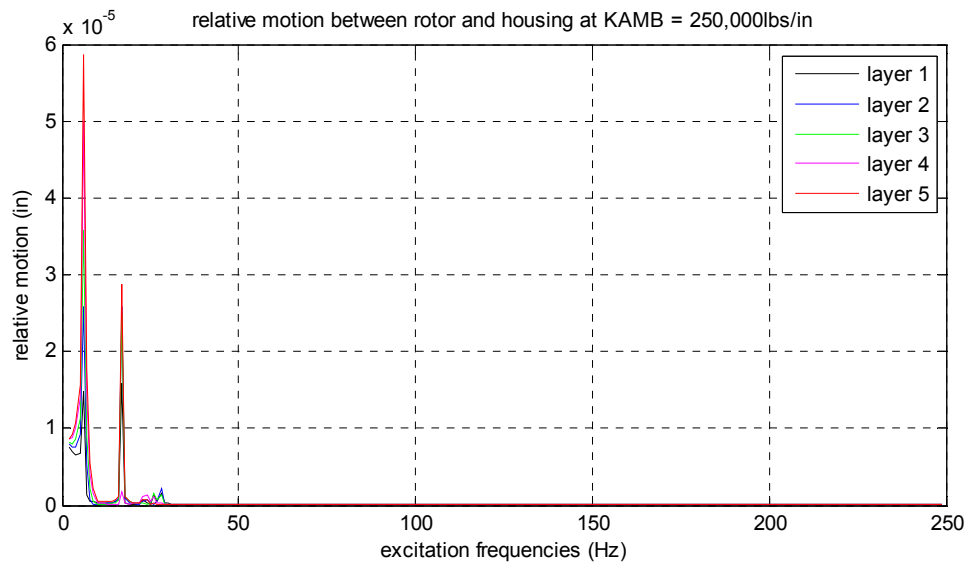


Fig. 13. Relative motion due to sinusoidal floor input in vertical direction from AAR's data at $K_{AMB} = 250,000 \text{ lbs/in}$

Check rotors' motion with respect to floor as shown in Fig. 14.

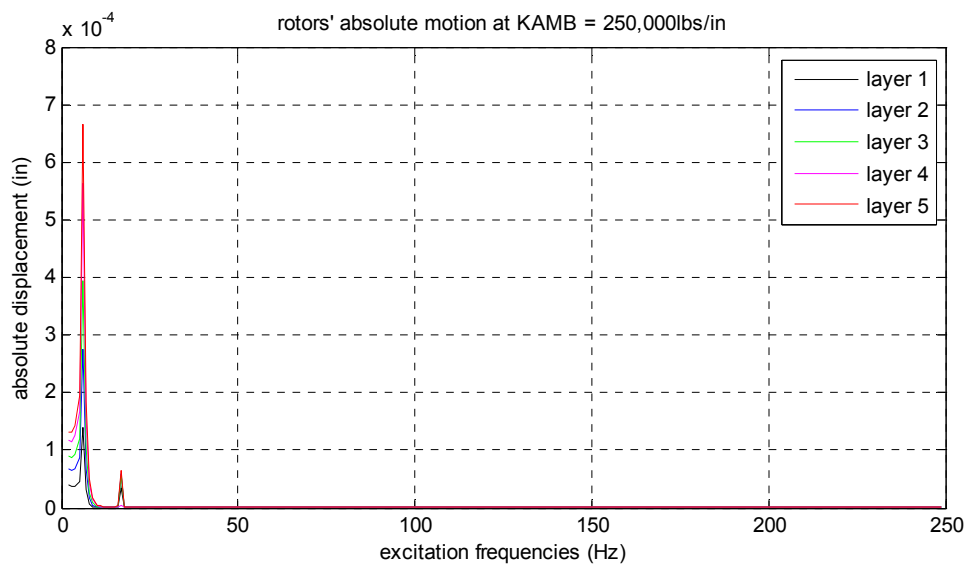


Fig. 14. Rotors' motion with respect to floor due to sinusoidal floor input in vertical direction from AAR's data at $K_{AMB} = 250,000 \text{ lbs/in}$

Notice that rotors' motion is fairly small compare with floor's input motion, which is in the order of 10^{-3} inch. Therefore, the vibration isolation system works well for sinusoidal floor input case at AMB stiffness 250,000 lbs/in.

3. MOTION ANALYSIS OF RAMP SUPPORT INPUT

3.1 Introduction

This kind of motion analysis is used to simulate the case when the locomotive approaches or leaves a bridge with a certain slope. Under this circumstance, the whole body model (including wheel suspension, bogie suspension and carriage) is utilized. Ramp support input model is shown in Fig. 15.

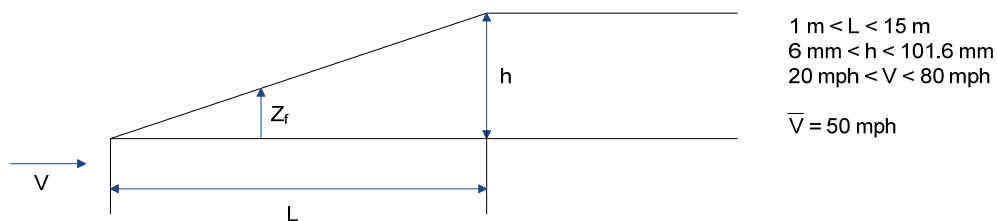
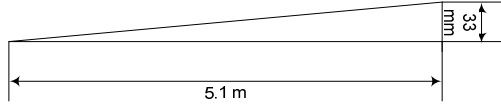


Fig. 15. Ramp support input model

From the data that AAR provided, the average bump slope reported from the test they conducted is 1:150 with a rise of 33 mm per 5.2 meters. The longest bump length that has been reported is about 15 meters. The range of bump lengths and bump heights from the survey is 1 meter to 15 meters and 6 mm to 101.6 mm, respectively. The train speed varies from 20 mph to 80 mph(Nicks 2009).

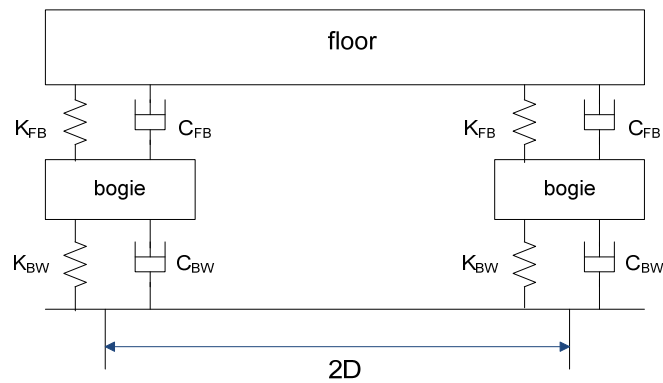
We use 50mph as the average speed and use 1:150 slope with bump length 5.1meters and bump height 33mm to do the simulation. Bump information is listed in Table 5.

Table 5. Bump information(Nicks 2009)

	Slope:	1:150
	Length:	5.1m
	Height:	33mm
	Speed:	22.2 m/s \approx 50 mph

3.2 Model setup

To rebuild the whole model, we need to add wheels and bogies into our original one. Additional model is shown in Fig. 16.

**Fig. 16.** Additional model setup(Park, et al. 2008)

3.3 Motion analysis

Let $z_{f1}(t)$, $z_{f2}(t)$ be the time varying input from wheel and rail interaction(as shown in Fig. 17), where $z_{f2}(t)$'s motion happens ahead of $z_{f1}(t)$. Write their expressions as follows:

$$z_{f2}(t) = \begin{cases} \frac{h}{L} \cdot V \cdot t, & t < t^* \\ h, & t \geq t^* \end{cases}$$

$$z_{f1}(t) = \begin{cases} 0, & t < \frac{2D}{V} \\ \frac{h}{L} \cdot V \cdot (t - \frac{2D}{V}), & \frac{2D}{V} \leq t < t^* + \frac{2D}{V} \\ h, & t \geq t^* + \frac{2D}{V} \end{cases} \quad (3.1)$$

Where $t^* = \frac{L}{V}$

Let $y_1(t)$, $y_2(t)$ be the motions of bogies, and $y_3(t)$, $\theta_3(t)$ be floor motions. Fig.

17 shows the motion assumptions.

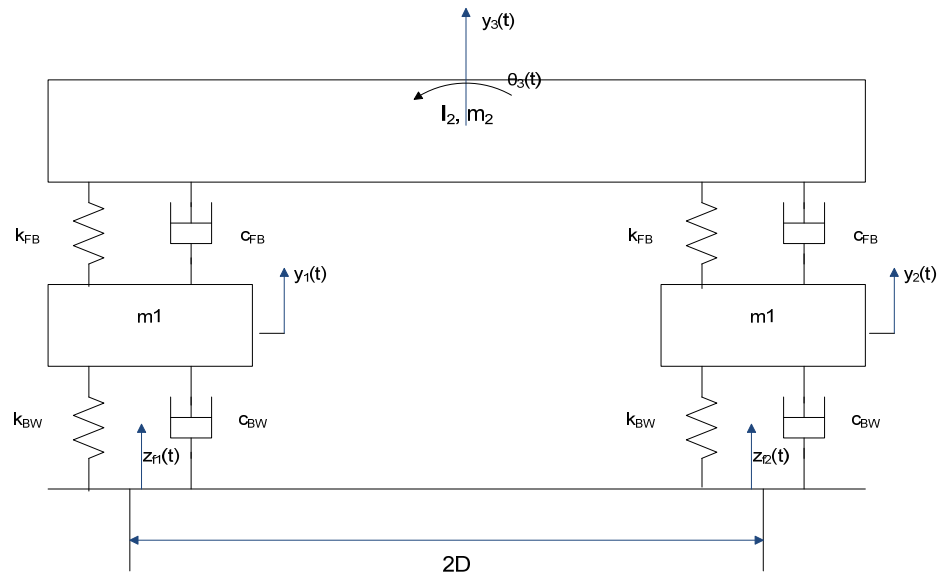


Fig. 17. Motion assumption of floor model

Parameters(Sun, et al. 2002):

Weight of the floor: $W = m_2 g = 128,772 \text{ lbs}$ ($m_2 = 333.6 \text{ lbs s}^2 / \text{in}$);

Then relate $y_3(t)$ and $\theta_3(t)$, which are floor motions, with previous EOM matrices (2.15) by replacing $z_f(t)$ with $y_3(t)$ and $\theta_{xf}(t)$ with $\theta_3(t)$. Let $\theta_{yf}(t) = 0$, leaving only input $z_{f1}(t)$ and $z_{f2}(t)$. The whole EOM matrices become:

$$\begin{aligned}
 & \begin{pmatrix} \ddot{Z}_1 \\ \ddot{Z}_{r1} \\ \vdots \\ \ddot{Z}_5 \\ \ddot{Z}_{r5} \\ \ddot{\theta}_{x1} \\ \ddot{\theta}_{y1} \\ \ddot{\theta}_{rx1} \\ \ddot{\theta}_{ry1} \\ \vdots \\ \ddot{\theta}_{x5} \\ \ddot{\theta}_{y5} \\ \ddot{\theta}_{rx5} \\ \ddot{\theta}_{ry5} \\ \ddot{y}_1 \\ \ddot{y}_2 \\ \ddot{y}_3 \\ \ddot{\theta}_3 \end{pmatrix}_{34 \times 1} \cdot \underline{\mathbf{M}}_{34 \times 34} + \begin{pmatrix} \dot{Z}_1 \\ \dot{Z}_{r1} \\ \vdots \\ \dot{Z}_5 \\ \dot{Z}_{r5} \\ \dot{\theta}_{x1} \\ \dot{\theta}_{y1} \\ \dot{\theta}_{rx1} \\ \dot{\theta}_{ry1} \\ \vdots \\ \dot{\theta}_{x5} \\ \dot{\theta}_{y5} \\ \dot{\theta}_{rx5} \\ \dot{\theta}_{ry5} \\ \dot{y}_1 \\ \dot{y}_2 \\ \dot{y}_3 \\ \dot{\theta}_3 \end{pmatrix}_{34 \times 1} \cdot \underline{\mathbf{C}}_{34 \times 34} + \begin{pmatrix} Z_1 \\ Z_{r1} \\ \vdots \\ Z_5 \\ Z_{r5} \\ \theta_{x1} \\ \theta_{y1} \\ \theta_{rx1} \\ \theta_{ry1} \\ \vdots \\ \theta_{x5} \\ \theta_{y5} \\ \theta_{rx5} \\ \theta_{ry5} \\ y_1 \\ y_2 \\ y_3 \\ \theta_3 \end{pmatrix}_{34 \times 1} \cdot \underline{\mathbf{K}}_{34 \times 34} = \begin{pmatrix} 0 \\ 0 \\ \vdots \\ 0 \\ 0 \\ 0 \\ 0 \\ 0 \\ 0 \\ \vdots \\ 0 \\ 0 \\ 0 \\ 0 \\ k_{BW} \cdot z_{f1}(t) + c_{BW} \cdot \dot{z}_{f1}(t) \\ k_{BW} \cdot z_{f2}(t) + c_{BW} \cdot \dot{z}_{f2}(t) \\ 0 \\ 0 \end{pmatrix}_{34 \times 1} \quad (3.7)
 \end{aligned}$$

$\underline{\mathbf{M}}$, $\underline{\mathbf{C}}$, $\underline{\mathbf{K}}$ matrices are listed in Appendix B; $z_{f1}(t)$, $z_{f2}(t)$ is defined in (3.1)

What we concern most is the relative motion of each layer (rotor to housing). By subtracting housing's motion from rotor's motion, their relative motion can be calculated, i.e. $Z_{r1}(t) - Z_1(t)$ is the vertical relative displacement between rotor_1 and housing_1. Furthermore, the largest relative motion, as defined in Fig. 9, can be written as (take the 1st layer for example) $Z_{r1}(t) - Z_1(t) + aa \cdot (\theta_{rx1}(t) - \theta_{x1}(t))$. Fig. 18 shows the

largest relative motion vs. time at 0 rad/sec. Fig. 19 shows the same plot at spin rate of 500 rad/sec.

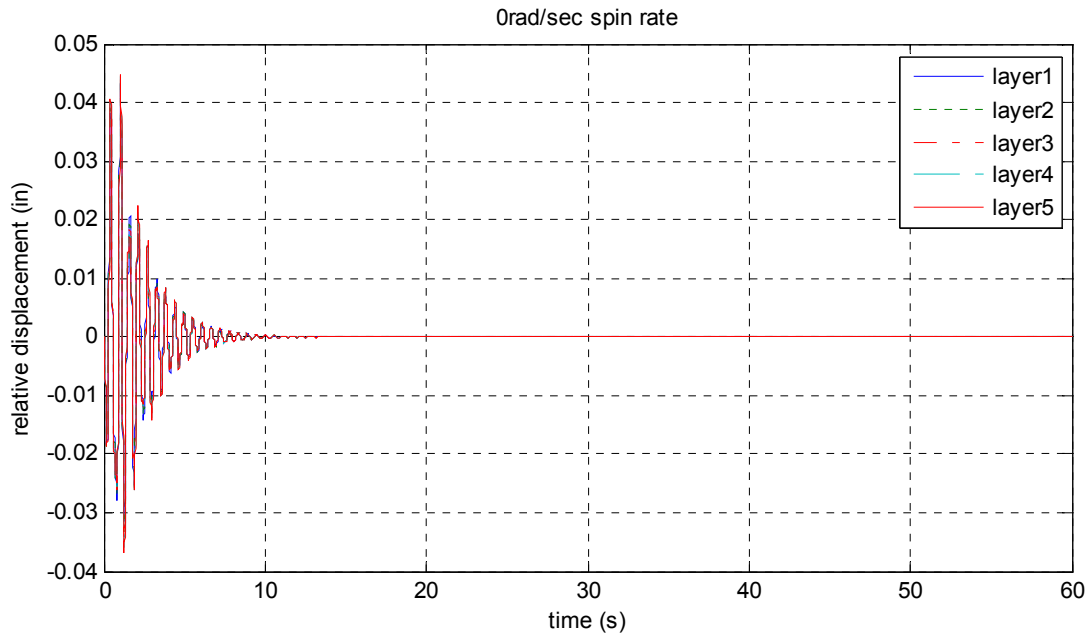


Fig. 18. Largest relative motion vs. time for ramp input without catcher bearing at 0 rad/sec

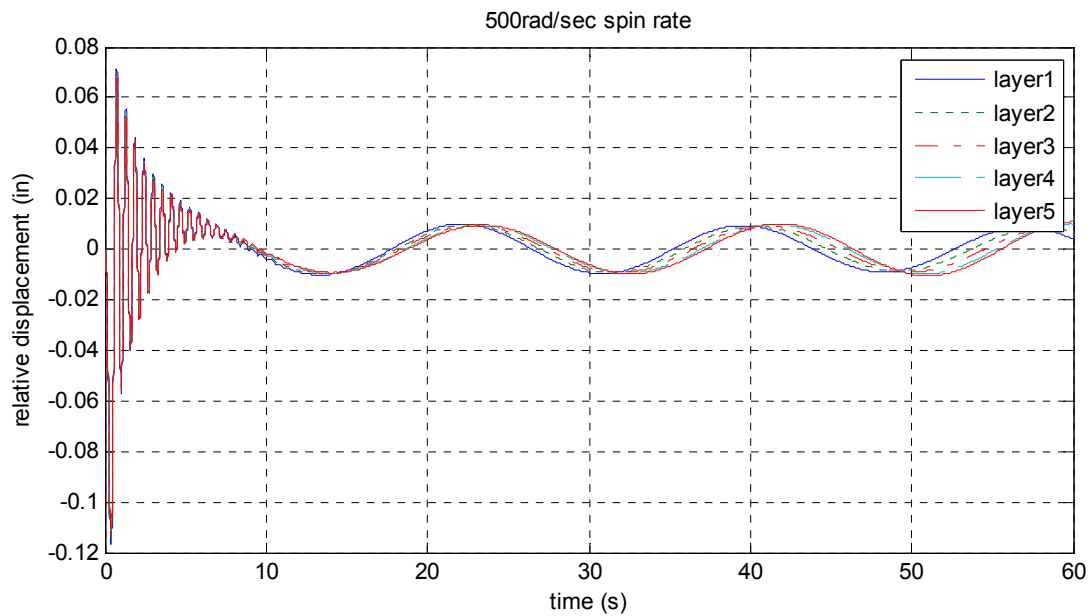


Fig. 19. Largest relative motion vs. time for ramp input without catcher bearing at 500 rad/sec

The duration of the train on the ramp is 0.64 second. As can be seen from Fig. 18, even at AMB stiffness 250,000 lbs/in, the maximum relative displacement is still up to 0.04 inch, while our allowed gap is 0.02 inch. From Fig. 19, the maximum relative displacement increases to 0.12 inch at 500 rad/sec spin rate and there is unexpected oscillation after the bump due to gyroscopic effect.

Basically, there are two ways to decrease the relative motion. One is to decrease the 1st layer isolators' stiffness so that the severe vibration on the floor will not propagate to its upper layers. The other is to increase AMBs' stiffness so that the motion difference between rotors and housings could be kept small.

Fig. 20 shows the maximum relative motion varying with the 1st layer isolators' stiffness from 1000 to 10⁶ lbs/in. We can see that by decreasing the stiffness of the 1st layer isolators, the maximum relative motion only improves a little, from 0.86 inch at 10⁶ lbs/in to 0.57 inch at 1000 lbs/in.

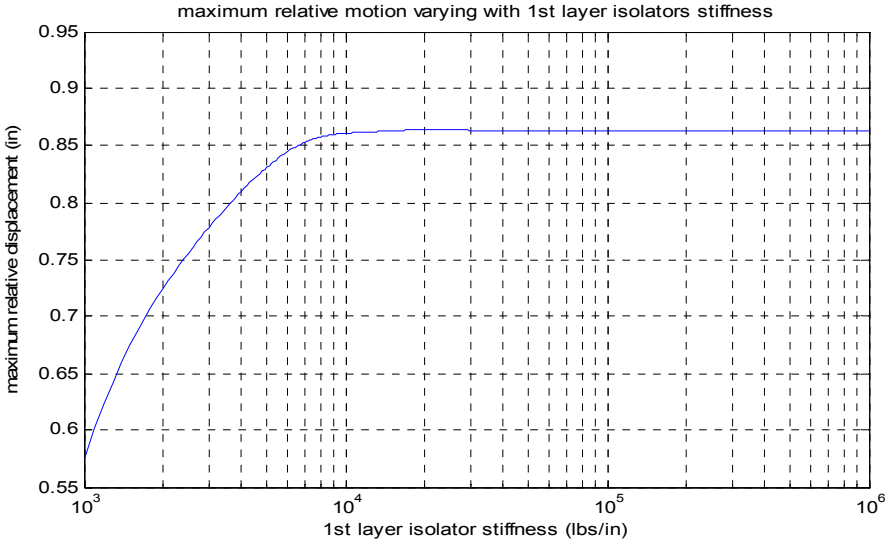


Fig. 20. Maximum relative motion vs. different stiffness of the 1st layer isolators

Fig. 21 shows the maximum relative motion with magnetic bearings' stiffness ranging from 1000 to 10^6 lb/in. By increasing the AMB stiffness, it helps a lot to reduce the maximum relative motion, from 0.85 inch at 1000 lb/in to less than 0.1 inch at 10^6 lb/in.

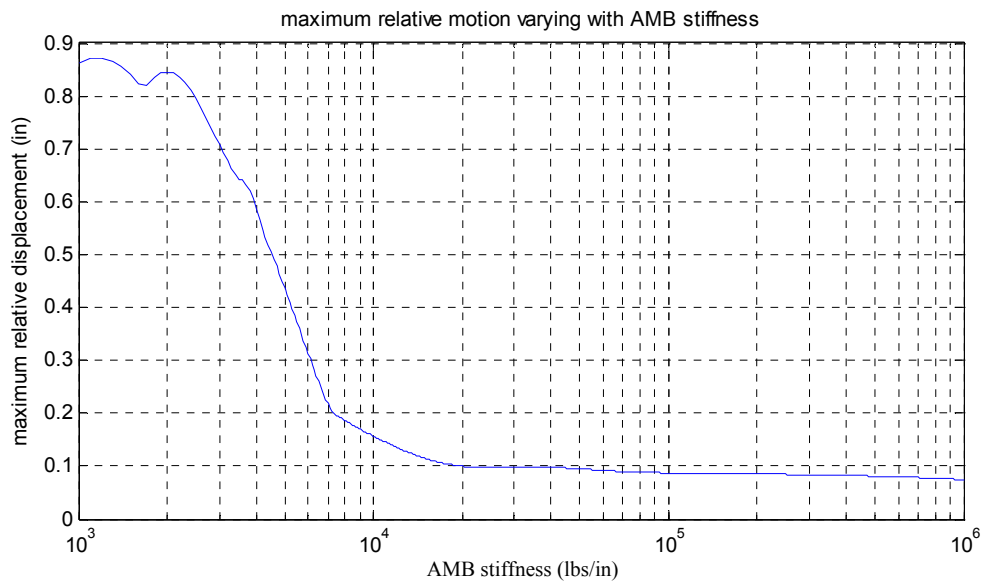


Fig. 21. Maximum relative motion vs. different AMB stiffness

Neither method would be able to decrease the maximum relative motion to 0.02 inch, which is the gap between AMB and rotor. Therefore, collisions between rotors and AMBs would happen if there is no protection in between. Catcher bearing(also known as Auxiliary Bearing or Back-up Bearing), provides a way to limit the motion of rotors so that when the relative displacement exceeds the gap between catcher bearings and rotors, these two would interact, protecting AMBs from colliding with rotors.

3.4 Model with catcher bearings

The setup model of catcher bearings is shown in Fig. 22 and Fig. 23. G_1, G_2, G_3, G_4 in yz plane and G_5, G_6, G_7, G_8 in xz plane are gaps between catcher bearings and rotors at eight locations. z_r, θ_r and z_h, θ_h are motions of rotor and housing, respectively. k_{cb}, c_{cb} are stiffness and damping of catcher bearing. (for illustration, only motions in yz plane are discussed in detail)

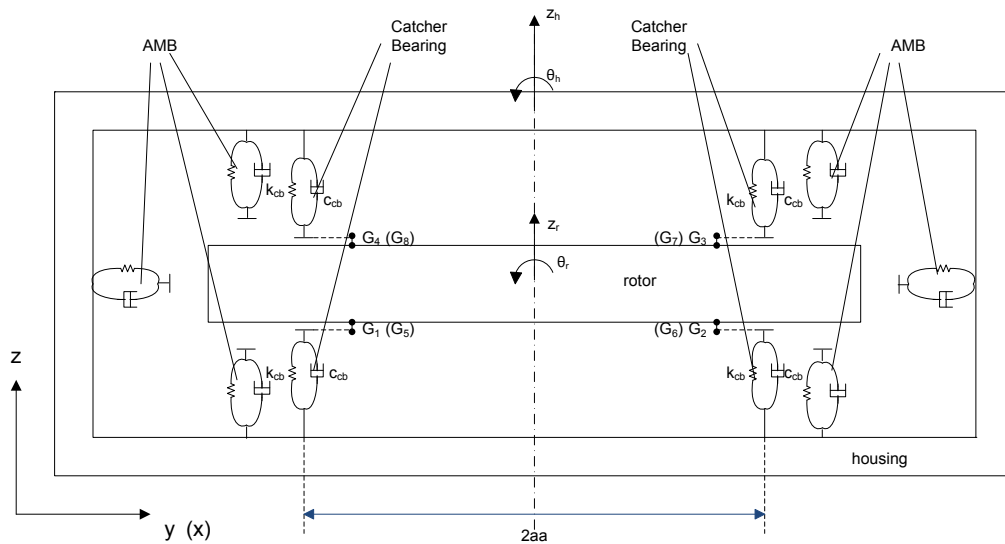


Fig. 22. Setup model with catcher bearings

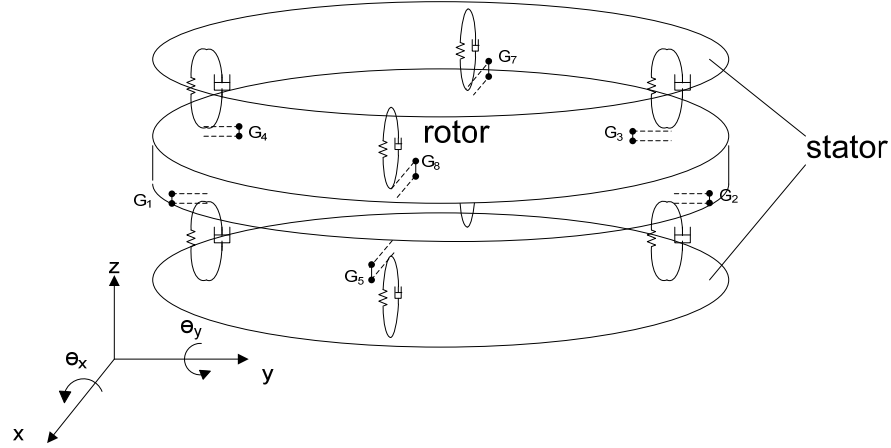


Fig. 23. 3-D illustration of the model with catcher bearings (spring and damper represents catcher bearing)

The condition for catcher bearing and rotor's interaction is when the largest relative motion exceeds the gap G_1 or G_2 or G_3 or G_4 , i.e. if

$$\Delta_3 = z_r - z_h + (\theta_r - \theta_h) \cdot aa > G_3 \quad (3.8)$$

Then the rotor and the catcher bearing at location G_3 will contact. The force of this interaction due to spring is written as

$$F_{3_k} = \begin{cases} k_{cb} \cdot (\Delta_3 - G_3), & \Delta_3 \geq G_3 \\ 0, & \Delta_3 < G_3 \end{cases} \quad (3.9)$$

The force due to damper is written as

$$F_{3_c} = \begin{cases} c_{cb} \cdot \dot{\Delta}_3, & \dot{\Delta}_3 \geq 0, \Delta_3 > G_3 \\ 0, & \dot{\Delta}_3 < 0 \end{cases} \quad (3.10)$$

So the total force

$$F_3 = F_{3_k} + F_{3_c} \quad (3.11)$$

The interactive forces are shown in Fig. 24, where F_3 is acting on housing and F_3' is acting on rotor. The total effects on rotor and housing are F_r , M_r and F_H , M_H , respectively. For this case,

$$\begin{aligned} F_H &= F_3 \\ M_H &= F_3 \cdot aa \\ F_r &= -F_H \\ M_r &= -M_H \end{aligned} \quad (3.12)$$

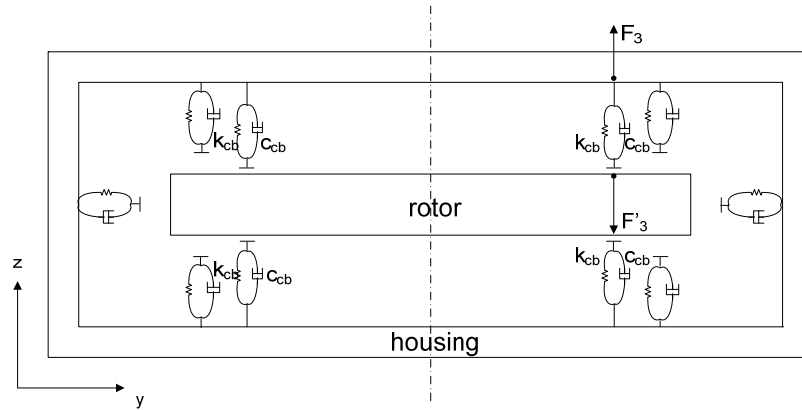


Fig. 24. Interactive forces on the rotor and housing

By adding statements in the code to determine the additional forces and torques, it is possible to figure out the interaction at certain time and its corresponding effects on the rotors and housings, which appear to be the external forces in the EOM Matrices.

Table 6. Parameters for catcher bearings

Stiffness k_{cb}	Damping c_{cb}	Distance from the center of the rotor aa	Gap $G_1, G_2, G_3,$ and G_4
10^6 lbs/in	450 lb*sec/in (with damping ratio 0.05)	20 inches	0.01 inch

Fig. 25, 26 shows the relative motion after adding catcher bearings to the system at zero spin velocity of rotors with AMB stiffness 1000 lbs/in and 250,000 lbs/in, respectively. Parameters for catcher bearings are listed in Table 6. As we can see, maximum relative motion is confined within 0.02 inch, which is the gap between rotors and AMBs. As the AMB stiffness increases, the interactive time between rotor and catcher bearing decreases. The maximum forces exerted on the catcher bearings at spin rate of 500 rad/sec with catcher bearing stiffness: 5,000,000 lbs/in are listed in Table 7.

Fig. 27 shows 1st layer's absolute motion at spin rate of 0 rad/sec.

Fig. 28 shows the relative motion at 500 rad/sec. As we can see, there are unexpected long-lasting oscillations remaining even after the bump. From the absolute motion plots of the first layer shown in Fig. 29, this can be explained by observing the oscillations of rotors' θ_x and θ_y motions. They can hardly be suppressed due to gyroscopic effects.

Fig. 30 and 31 show this oscillation can be suppressed by increasing the stiffness of the AMBs. Fig. 32 shows the oscillation dissipates more quickly when damping increases. Therefore, it is recommended that AMBs are stiff and have large damping ratio for ramp support input.

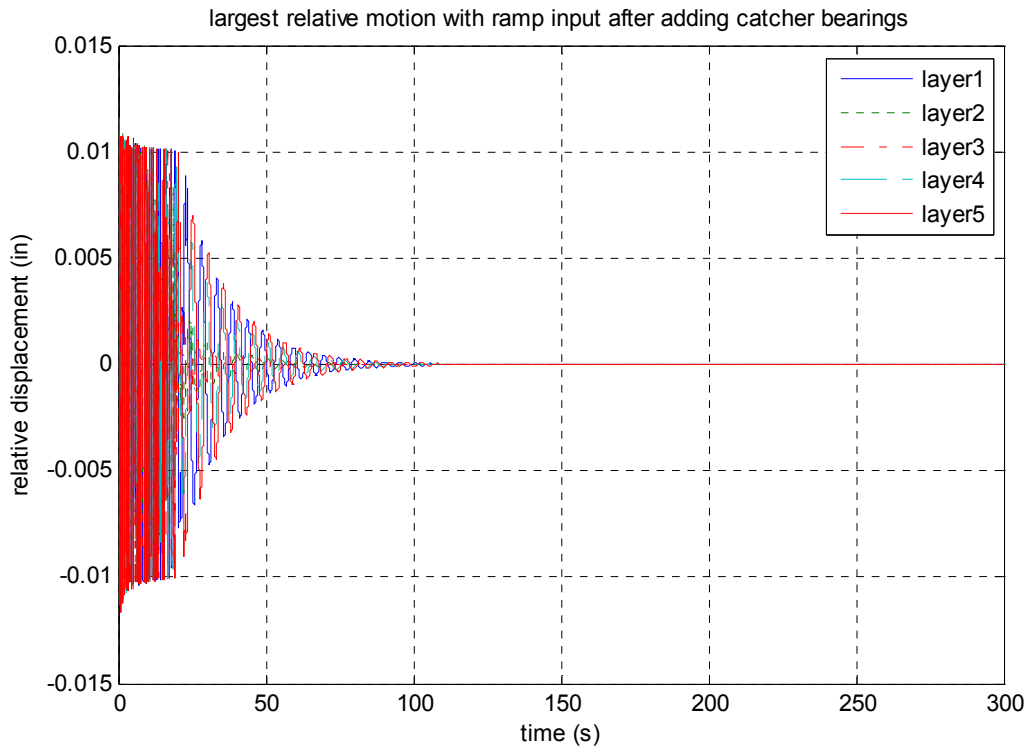


Fig. 25. Relative motion with catcher bearings

(AMB stiffness: 1,000 lbs/in; AMB damping ratio: 0.05; catcher bearing stiffness: 1,000,000 lbs/in; catcher bearing damping: 450 lb sec/in; rotors' spin velocity: 0 rad/sec)

Table 7. Maximum deflections and forces in catcher bearings

(AMB stiffness: 250,000 lbs/in; AMB damping ratio: 0.05; catcher bearing stiffness: 5,000,000 lbs/in; catcher bearing damping: 450 lb sec/in; rotors' spin velocity: 500 rad/sec)

	Layer 1	Layer 2	Layer 3	Layer 4	Layer 5
Max. deflection in catcher bearing	0.0124 (in)	0.0123 (in)	0.0128 (in)	0.0136 (in)	0.0136 (in)
Max. force in catcher bearing	11987 (lbs)	11701 (lbs)	14078 (lbs)	18528 (lbs)	17915 (lbs)

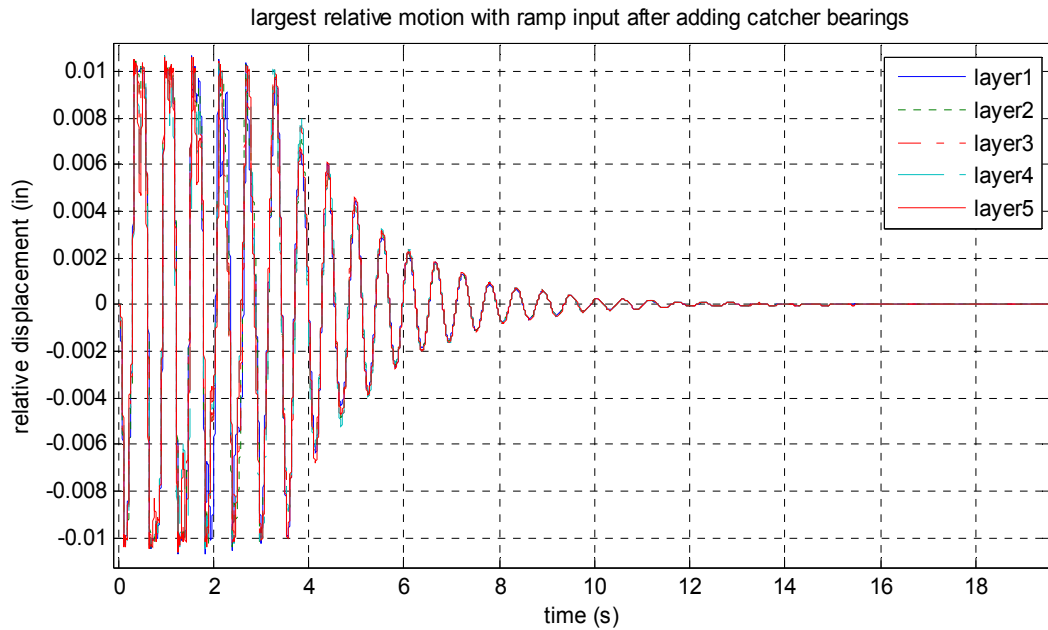


Fig. 26. Relative motion with catcher bearings
 (AMB stiffness: 250,000 lbs/in; AMB damping ratio: 0.05; catcher bearing stiffness: 1,000,000 lbs/in;
 catcher bearing damping: 450 lb sec/in; rotors' spin velocity: 0 rad/sec)

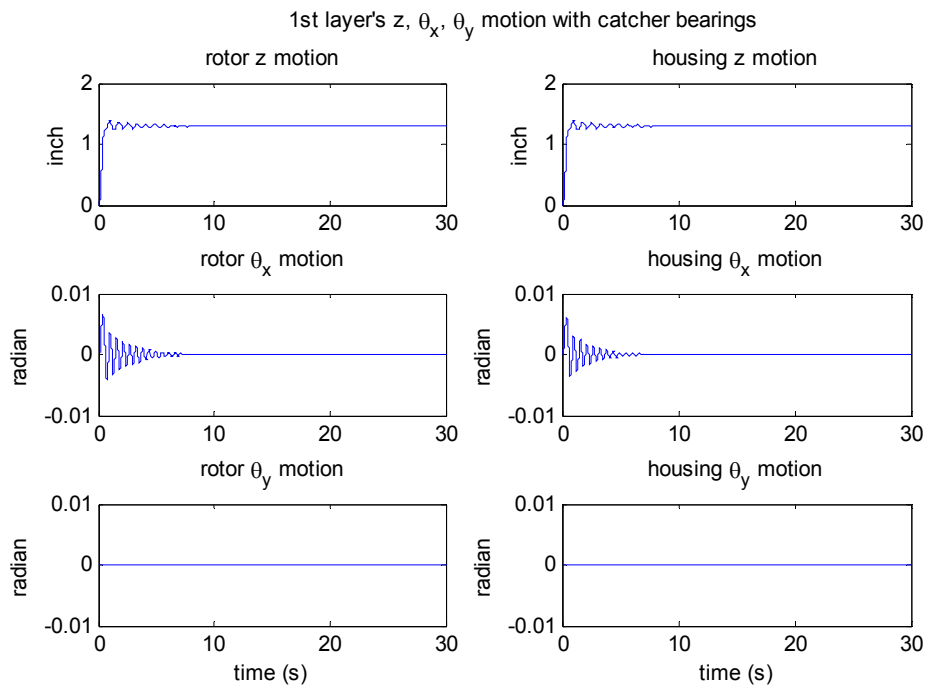


Fig. 27. 1st layer's absolute motion with catcher bearings
 (AMB stiffness: 250,000 lbs/in; AMB damping ratio: 0.05; rotors' spin velocity: 0 rad/sec)

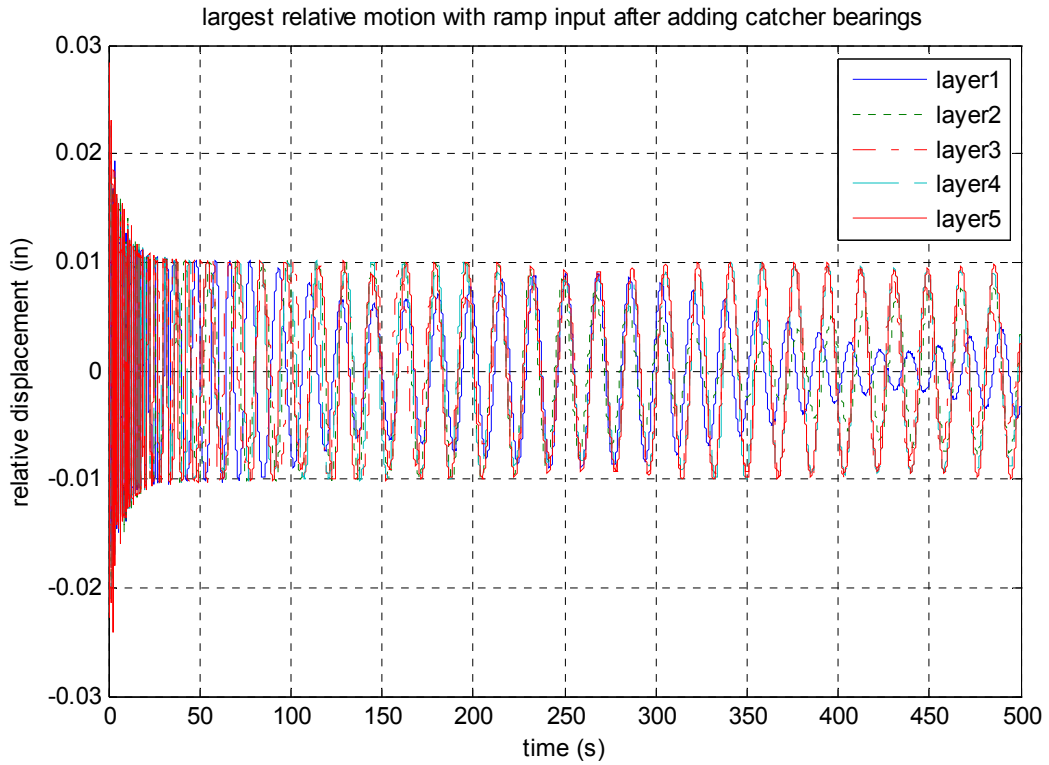


Fig. 28. Relative motion with catcher bearings
 (AMB stiffness: 250,000 lbs/in; AMB damping ratio: 0.05; rotors' spin velocity: 500 rad/sec)

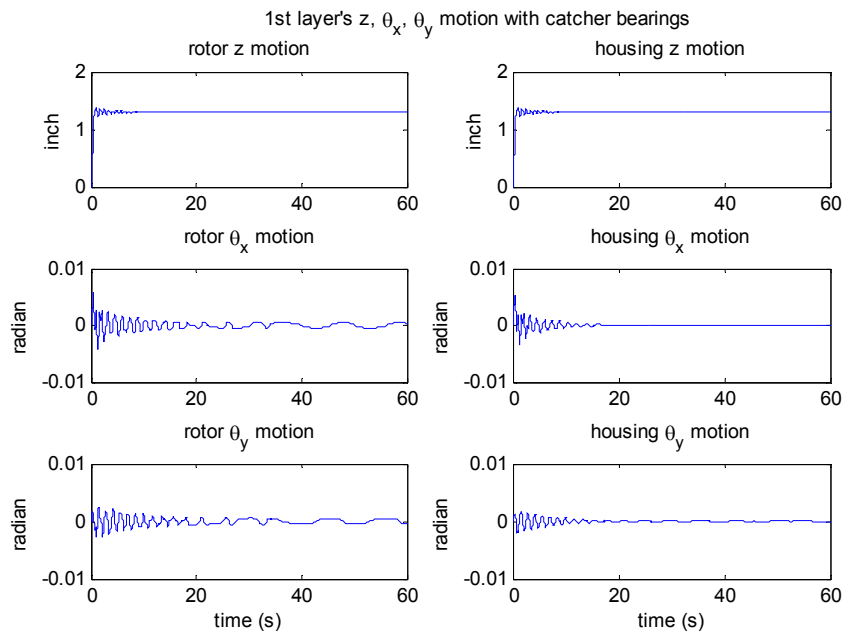


Fig. 29. 1st layer's absolute motions with catcher bearings
 (AMB stiffness: 250,000 lbs/in; AMB damping ratio: 0.05; rotors' spin velocity: 500 rad/sec)

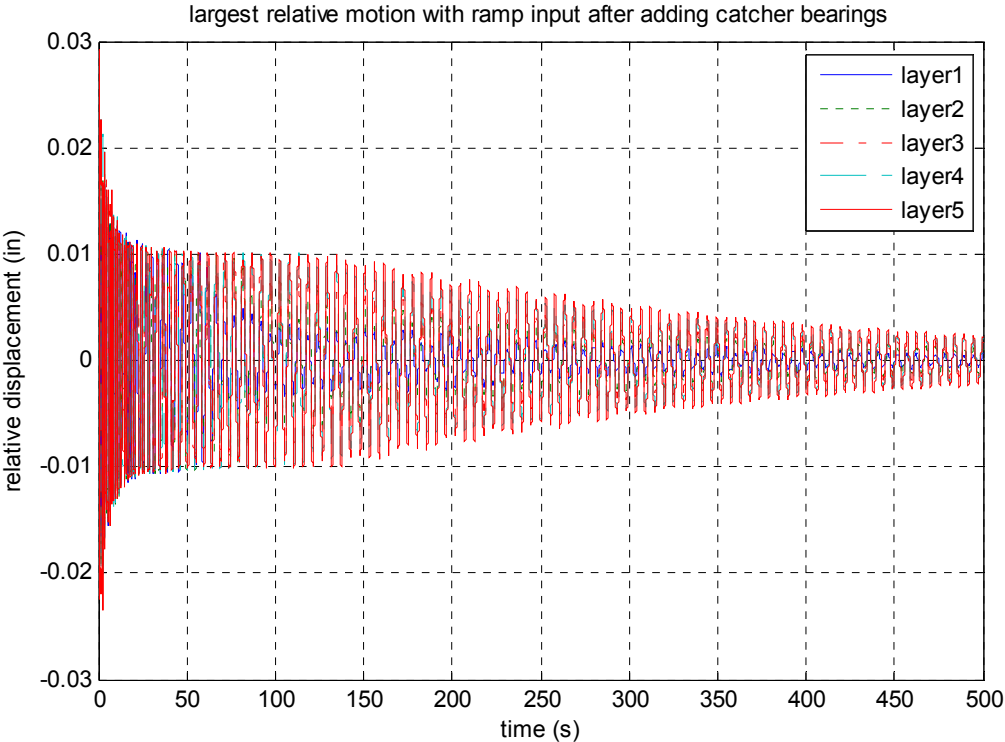


Fig. 30. Relative motion with catcher bearings
(AMB stiffness: 1,000,000 lbs/in; AMB damping ratio: 0.05; rotors' spin velocity: 500 rad/sec)

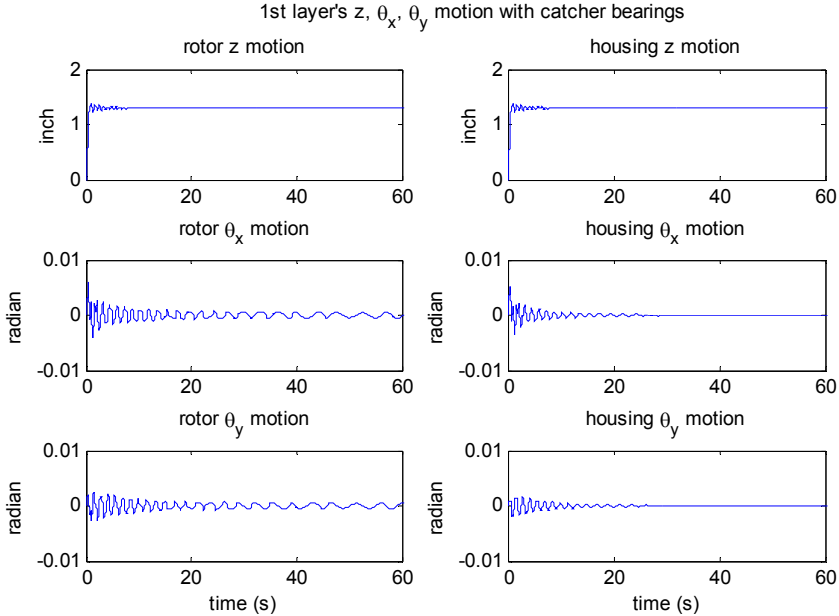


Fig. 31. 1st layer's absolute motions with catcher bearings
(AMB stiffness: 1,000,000 lbs/in; AMB damping ratio: 0.05; rotors' spin velocity: 500 rad/sec)

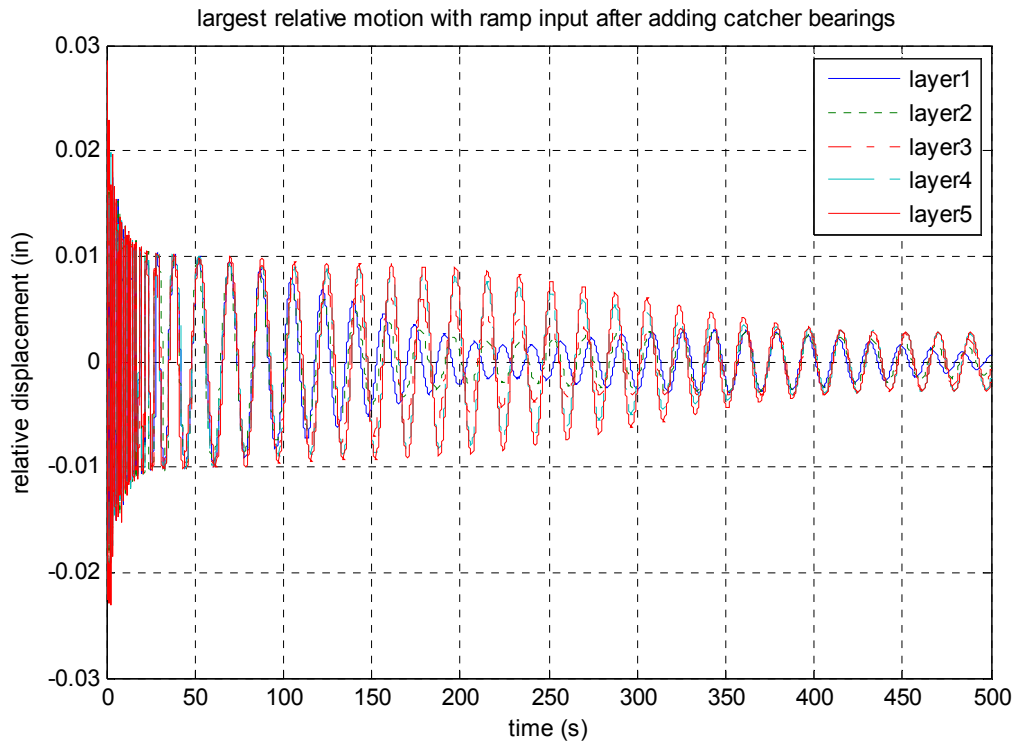


Fig. 32. Relative motion with catcher bearings
(AMB stiffness: 250,000 lbs/in; AMB damping ratio: 0.3; rotors' spin velocity: 500 rad/sec)

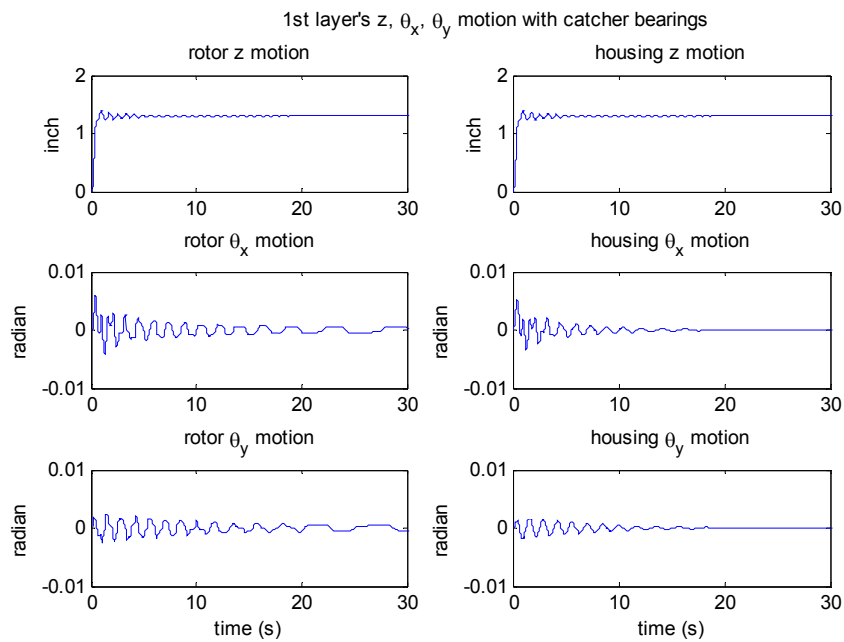


Fig. 33. 1st layer's absolute motions with catcher bearings
(AMB stiffness: 1,000,000 lbs/in; AMB damping ratio: 0.3; rotors' spin velocity: 500 rad/sec)

4. DE-LEVITATION METHOD WITH RAMP INPUT

4.1 Introduction

During bumps, we limited the rotors' motion by introducing catcher bearings in order to protect AMBs. As we can see from simulation results, the motions of rotors are indeed confined within the safe space. However, the down side is also obvious if rotors are spinning during bumps. The gyroscopic effects are so strong that the pitching and rolling of rotors could still excite the oscillation and even cause contact between rotors and catcher bearings after bumps as we can see from Fig. 30. Increasing the AMB stiffness and damping might be one solution to suppress gyroscopic effects. But for high spin rate (in our case is 500 rad/sec), as shown in Fig. 21, AMB stiffness would never be high enough to limit the maximum relative motion within 0.02 inch safe space.

Another reasonable solution is de-levitation. As the train approaches the bump, we first de-levitate the rotors by decreasing the magnetic force slowly. Then apply another downward magnetic force to make sure that rotors would sit on the Catcher Bearings during the bump. After the bump, rotors are levitated by AMBs. As it turned out, de-levitation provides a way to overcome the unexpected oscillation induced by gyroscopic.

4.2 Model set up

Since de-levitation is required to turn off all the support forces from AMBs during bumps. Without these magnetic forces, we spared the anxiety of modeling AMBs. However, the difficulty of simulating this interaction process is, there are three circumstances to consider: contact between rotor and lower catcher bearings, no contact,

and contact between rotor and upper catcher bearings. To include all these circumstances, codes for judging different conditions need to be added in the integration sub-function.

The set-up model for one layer is illustrated in Fig. 34. Define new reference position EP, which is the position where rotor and catcher bearings just contact (or just lose contact). Floor-bogie-wheel model is the same as the one in Fig. 13 and 14.

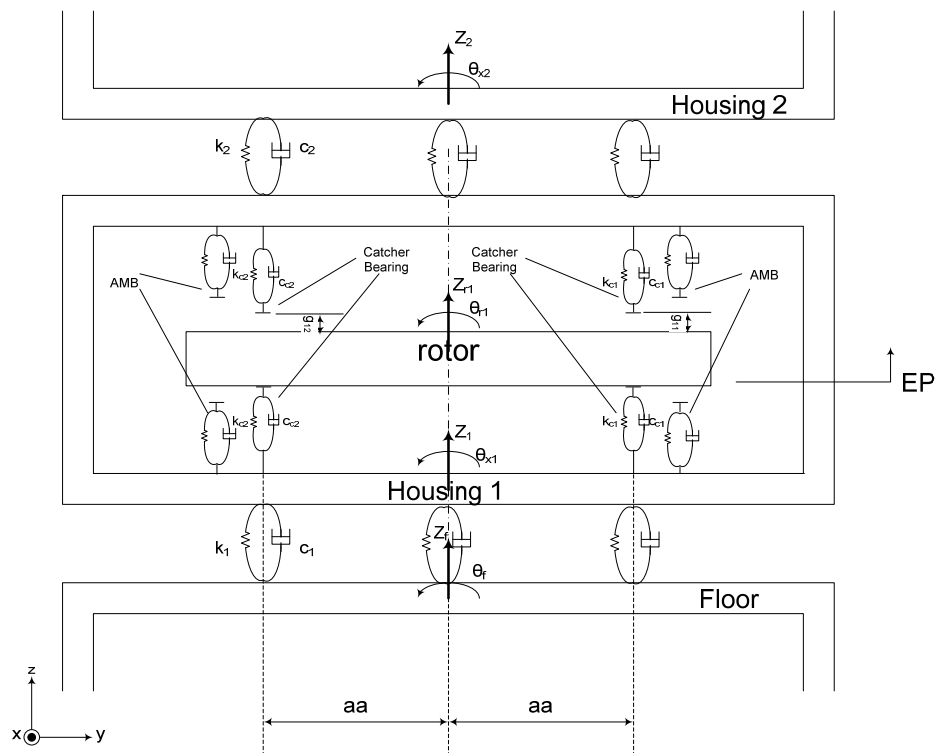


Fig. 34. One layer of de-levitation model on yz plane

Fig. 35 illustrates the whole model for the simulation and Table 8 lists main parameters for the whole model.

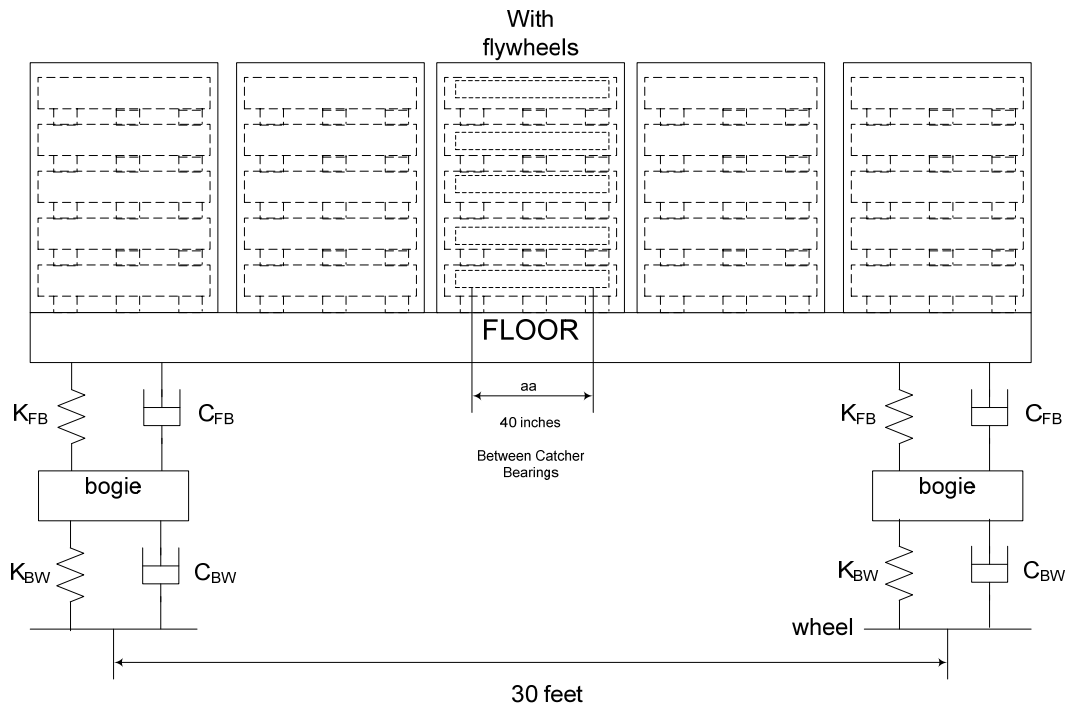


Fig. 35. Whole model for the simulation

Table 8. Main parameters for de-levitating model(*data is from Sun, et al. 2002)

Weight	Rotor	8000 lbs
	Housing	4000 lbs
	Floor(Wagon body mass-loaded*)	128772 lbs
	Bogie*	8000 lbs
	Downward magnetic force	7500 lbs
Mass moment of inertial (along x axis)	Rotor	8500 lbs s ² in
	Housing	8500 lbs s ² in
	Floor(Wagon*)	5.4×10 ⁶ lbs s ² in
Stiffness	Catcher Bearing	10 ⁶ lbs/in
	one isolator	53046 lbs/in
	Floor and bogie	14859 lbs/in
	Bogie and wheel	37148 lbs/in
Damping	Catcher bearing	455 lb sec/in
	One isolator	258 ~ 116 lb sec/in
	Floor and bogie	171 lb sec/in
	Bogie and wheel	57 lb sec/in
Gap	Rotor and upper Catcher Bearing	0.02 inch

Notations:

m_1 : mass of bogie

m_f : mass of floor

I_2 : mass moment of inertia of floor along x axis

m_{r1} : mass of rotor

m_1 : mass of housing 1

I_{rx1} : mass moment of inertia of rotor 1 along x axis

I_{x1} : mass moment of inertia of housing 1 along x axis

I_{ry1} : mass moment of inertia of rotor 1 along y axis

I_{y1} : mass moment of inertia of housing 1 along y axis

W_R : weight of a rotor

F_m : downward magnetic force on the rotor

k_{c11} , k_{c12} : right and left catcher bearings' (on yz plane) stiffness

k_{c11_y} , k_{c12_y} : right and left catcher bearings' (on xz plane) stiffness

c_{c11} , c_{c12} : right and left catcher bearings' (on yz plane) damping

c_{c11_y} , c_{c12_y} : right and left catcher bearings' (on xz plane) damping

k_1 , k_2 : first and second layers' isolator stiffness

c_1 , c_2 : first and second layers' isolator damping

g_{11} : right hand side gap between rotor and upper catcher bearings at EP

g_{12} : left hand side gap between rotor and upper catcher bearings at EP

4.3 Motion analysis

For housing 1, using Newton's law $F = ma$:

$$\begin{aligned}
m_1 \ddot{Z}_1 = & Kc11 \cdot (Z_{r1} + \theta_{rx1} \cdot aa - Z_1 - \theta_{x1} \cdot aa - g11) + Cc11 \cdot (\dot{Z}_{r1} + \dot{\theta}_{rx1} \cdot aa - \dot{Z}_1 - \dot{\theta}_{x1} \cdot aa) \\
& + Kc12 \cdot (Z_{r1} - \theta_{rx1} \cdot aa - Z_1 + \theta_{x1} \cdot aa - g12) + Cc12 \cdot (\dot{Z}_{r1} - \dot{\theta}_{rx1} \cdot aa - \dot{Z}_1 + \dot{\theta}_{x1} \cdot aa) \\
& + Kc11_y \cdot (Z_{r1} + \theta_{ry1} \cdot aa - Z_1 - \theta_{y1} \cdot aa - g11_y) + Cc11_y \cdot (\dot{Z}_{r1} + \dot{\theta}_{ry1} \cdot aa - \dot{Z}_1 - \dot{\theta}_{y1} \cdot aa) \\
& + Kc12_y \cdot (Z_{r1} - \theta_{ry1} \cdot aa - Z_1 + \theta_{y1} \cdot aa - g12_y) + Cc12 \cdot (\dot{Z}_{r1} - \dot{\theta}_{ry1} \cdot aa - \dot{Z}_1 + \dot{\theta}_{y1} \cdot aa) \\
& + 3 \cdot K_2 \cdot (Z_2 + \theta_2 \cdot aa - Z_1 - \theta_1 \cdot aa) + 3 \cdot C_2 \cdot (\dot{Z}_2 + \dot{\theta}_2 \cdot aa - \dot{Z}_1 - \dot{\theta}_1 \cdot aa) \\
& + 2 \cdot K_2 \cdot (Z_2 - Z_1) + 2 \cdot C_2 \cdot (\dot{Z}_2 - \dot{Z}_1) \\
& + 3 \cdot K_2 \cdot (Z_2 - \theta_2 \cdot aa - Z_1 + \theta_1 \cdot aa) + 3 \cdot C_2 \cdot (\dot{Z}_2 - \dot{\theta}_2 \cdot aa - \dot{Z}_1 + \dot{\theta}_1 \cdot aa) \\
& - 3 \cdot K_1 \cdot (Z_1 + \theta_1 \cdot aa - Z_f - \theta_f \cdot aa) - 3 \cdot C_1 \cdot (\dot{Z}_1 + \dot{\theta}_1 \cdot aa - \dot{Z}_f - \dot{\theta}_f \cdot aa) \\
& - 2 \cdot K_1 \cdot (Z_1 - Z_f) - 2 \cdot C_1 \cdot (\dot{Z}_1 - \dot{Z}_f) \\
& - 3 \cdot K_1 \cdot (Z_1 - \theta_1 \cdot aa - Z_f + \theta_f \cdot aa) - 3 \cdot C_1 \cdot (\dot{Z}_1 - \dot{\theta}_1 \cdot aa - \dot{Z}_f + \dot{\theta}_f \cdot aa)
\end{aligned} \tag{4.1}$$

Where, g11, g12 are the right and left gap between upper Catcher Bearings and rotor.

If rotor and lower Catcher Bearings remain contact, then g11 and g12 in (4.1) should be set to 0; if rotor and Catcher Bearing lose contact, then the corresponding Kc and Cc in that layer should be set to 0, as well as g11 and g12; if rotor and upper Catcher Bearings contact, then g11 and g12 equal to the gap, which is 0.02 inch. These 3 cases should be considered during the simulation. The equations of motion are as follows.

For rotor 1:

$$\begin{aligned}
m_{r1} \cdot \ddot{Z}_{r1} = & -Fm - W_r \\
& - Kc11 \cdot (Z_{r1} + \theta_{rx1} \cdot aa - Z_1 - \theta_{x1} \cdot aa - g11) - Cc11 \cdot (\dot{Z}_{r1} + \dot{\theta}_{rx1} \cdot aa - \dot{Z}_1 - \dot{\theta}_{x1} \cdot aa) \\
& - Kc12 \cdot (Z_{r1} - \theta_{rx1} \cdot aa - Z_1 + \theta_{x1} \cdot aa - g12) - Cc12 \cdot (\dot{Z}_{r1} - \dot{\theta}_{rx1} \cdot aa - \dot{Z}_1 + \dot{\theta}_{x1} \cdot aa) \\
& - Kc11_y \cdot (Z_{r1} + \theta_{ry1} \cdot aa - Z_1 - \theta_{y1} \cdot aa - g11_y) - Cc11_y \cdot (\dot{Z}_{r1} + \dot{\theta}_{ry1} \cdot aa - \dot{Z}_1 - \dot{\theta}_{y1} \cdot aa) \\
& - Kc12_y \cdot (Z_{r1} - \theta_{ry1} \cdot aa - Z_1 + \theta_{y1} \cdot aa - g12_y) - Cc12_y \cdot (\dot{Z}_{r1} - \dot{\theta}_{ry1} \cdot aa - \dot{Z}_1 + \dot{\theta}_{y1} \cdot aa)
\end{aligned} \tag{4.2}$$

For housing 1's θ_x motion (θ_y motion are similar to their θ_x motion.), using $M = I\alpha$:

$$\begin{aligned}
I_{x1} \cdot \ddot{\theta}_{x1} = & aa \cdot [Kc11 \cdot (Z_{r1} + \theta_{rx1} \cdot aa - Z_1 - \theta_{x1} \cdot aa - g11) + Cc11 \cdot (\dot{Z}_{r1} + \dot{\theta}_{r1} \cdot aa - \dot{Z}_1 - \dot{\theta}_1 \cdot aa)] \\
& - aa \cdot [Kc12 \cdot (Z_{r1} - \theta_{rx1} \cdot aa - Z_1 + \theta_{x1} \cdot aa - g12) + Cc12 \cdot (\dot{Z}_{r1} - \dot{\theta}_{r1} \cdot aa - \dot{Z}_1 + \dot{\theta}_1 \cdot aa)] \\
& + aa \cdot [K_1 \cdot (Z_1 - \theta_{x1} \cdot aa - \theta_{y1} \cdot aa - Z_f + \theta_f \cdot aa) + C_1 \cdot (\dot{Z}_1 - \dot{\theta}_{x1} \cdot aa - \dot{\theta}_{y1} \cdot aa - \dot{Z}_f + \dot{\theta}_f \cdot aa)] \\
& + aa \cdot [K_1 \cdot (Z_1 - \theta_{x1} \cdot aa - Z_f + \theta_f \cdot aa) + C_1 \cdot (\dot{Z}_1 - \dot{\theta}_{x1} \cdot aa - \dot{Z}_f + \dot{\theta}_f \cdot aa)] \\
& + aa \cdot [K_1 \cdot (Z_1 - \theta_{x1} \cdot aa + \theta_{y1} \cdot aa - Z_f + \theta_f \cdot aa) + C_1 \cdot (\dot{Z}_1 - \dot{\theta}_{x1} \cdot aa + \dot{\theta}_{y1} \cdot aa - \dot{Z}_f + \dot{\theta}_f \cdot aa)] \\
& - aa \cdot [K_1 \cdot (Z_1 + \theta_{x1} \cdot aa - \theta_{y1} \cdot aa - Z_f - \theta_f \cdot aa) + C_1 \cdot (\dot{Z}_1 + \dot{\theta}_{x1} \cdot aa - \dot{\theta}_{y1} \cdot aa - \dot{Z}_f - \dot{\theta}_f \cdot aa)] \\
& - aa \cdot [K_1 \cdot (Z_1 + \theta_{x1} \cdot aa - Z_f - \theta_f \cdot aa) + C_1 \cdot (\dot{Z}_1 + \dot{\theta}_{x1} \cdot aa - \dot{Z}_f - \dot{\theta}_f \cdot aa)] \\
& - aa \cdot [K_1 \cdot (Z_1 + \theta_{x1} \cdot aa + \theta_{y1} \cdot aa - Z_f - \theta_f \cdot aa) + C_1 \cdot (\dot{Z}_1 + \dot{\theta}_{x1} \cdot aa + \dot{\theta}_{y1} \cdot aa - \dot{Z}_f - \dot{\theta}_f \cdot aa)] \\
& + aa \cdot [K_2 \cdot (Z_2 + \theta_{x2} \cdot aa - \theta_{y2} \cdot aa - Z_1 - \theta_{x1} \cdot aa + \theta_{y1} \cdot aa) + C_2 \cdot (\dot{Z}_2 + \dot{\theta}_{x2} \cdot aa - \dot{\theta}_{y2} \cdot aa - \dot{Z}_1 - \dot{\theta}_{x1} \cdot aa + \dot{\theta}_{y1} \cdot aa)] \\
& + aa \cdot [K_2 \cdot (Z_2 + \theta_{x2} \cdot aa - Z_1 - \theta_{x1} \cdot aa) + C_2 \cdot (\dot{Z}_2 + \dot{\theta}_{x2} \cdot aa - \dot{Z}_1 - \dot{\theta}_{x1} \cdot aa)] \\
& + aa \cdot [K_2 \cdot (Z_2 + \theta_{x2} \cdot aa + \theta_{y2} \cdot aa - Z_1 - \theta_{x1} \cdot aa - \theta_{y1} \cdot aa) + C_2 \cdot (\dot{Z}_2 + \dot{\theta}_{x2} \cdot aa + \dot{\theta}_{y2} \cdot aa - \dot{Z}_1 - \dot{\theta}_{x1} \cdot aa - \dot{\theta}_{y1} \cdot aa)] \\
& - aa \cdot [K_2 \cdot (Z_2 - \theta_{x2} \cdot aa - \theta_{y2} \cdot aa - Z_1 + \theta_{x1} \cdot aa + \theta_{y1} \cdot aa) + C_2 \cdot (\dot{Z}_2 - \dot{\theta}_{x2} \cdot aa - \dot{\theta}_{y2} \cdot aa - \dot{Z}_1 + \dot{\theta}_{x1} \cdot aa + \dot{\theta}_{y1} \cdot aa)] \\
& - aa \cdot [K_2 \cdot (Z_2 - \theta_{x2} \cdot aa - Z_1 + \theta_{x1} \cdot aa) + C_2 \cdot (\dot{Z}_2 - \dot{\theta}_{x2} \cdot aa - \dot{Z}_1 + \dot{\theta}_{x1} \cdot aa)] \\
& - aa \cdot [K_2 \cdot (Z_2 - \theta_{x2} \cdot aa + \theta_{y2} \cdot aa - Z_1 + \theta_{x1} \cdot aa - \theta_{y1} \cdot aa) + C_2 \cdot (\dot{Z}_2 - \dot{\theta}_{x2} \cdot aa + \dot{\theta}_{y2} \cdot aa - \dot{Z}_1 + \dot{\theta}_{x1} \cdot aa - \dot{\theta}_{y1} \cdot aa)]
\end{aligned}
\tag{4.3}$$

For rotor 1's θ_x motion:

$$\begin{aligned}
I_{rx1} \cdot \ddot{\theta}_{rx1} + (I_p \cdot \omega) \cdot \dot{\theta}_{ry1} = & -aa \cdot [Kc11 \cdot (Z_{r1} + \theta_{rx1} \cdot aa - Z_1 - \theta_{x1} \cdot aa - g11) + Cc11 \cdot (\dot{Z}_{r1} + \dot{\theta}_{rx1} \cdot aa - \dot{Z}_1 - \dot{\theta}_{x1} \cdot aa)] \\
& + aa \cdot [Kc12 \cdot (Z_{r1} - \theta_{rx1} \cdot aa - Z_1 + \theta_{x1} \cdot aa - g12) + Cc12 \cdot (\dot{Z}_{r1} - \dot{\theta}_{rx1} \cdot aa - \dot{Z}_1 + \dot{\theta}_{x1} \cdot aa)]
\end{aligned}
\tag{4.4}$$

For the whole setup (Fig. 35), differential equations can be written in the following

matrix form:

$ \begin{matrix} m & m_r & \dots & m \\ \vdots & \vdots & & \vdots \\ I_x & I_y & I_{xy} & \dots & I_x & I_y & I_{xy} & \dots & I_x & I_y & I_{xy} \\ \vdots & \vdots & \vdots & \vdots & \vdots & \vdots & \vdots & \vdots & \vdots & \vdots & \vdots \\ m_1 & m_2 & \dots & m_1 & m_2 & \dots & m_1 & m_2 & \dots & m_1 & m_2 \end{matrix} $	$ \begin{matrix} 8k1+8k2+k11+\dots+k12_y \\ \vdots \\ 0 & 0 & -8k1 & 0 \end{matrix} $	$ \begin{matrix} Z_1 \\ Z_2 \\ \vdots \\ Z_5 \\ Z_6 \\ \theta_A \\ \theta_B \\ \theta_{rd} \\ \theta_{ps} \\ \vdots \\ \theta_{ps} \\ \theta_{ps} \\ \theta_{ps} \\ \theta_{ps} \\ \theta_{ps} \\ \theta_{ps} \\ \theta_{ps} \\ y_1 \\ y_2 \\ \theta_2 \dots \theta_{34} \end{matrix} $
$ \begin{matrix} 6k1 \cdot a^2 + 6k2 \cdot a^2 + \dots \\ 0 \\ -(k11+k12) \cdot a^2 \\ 0 \\ 6k1 \cdot b^2 + 6k2 \cdot b^2 + \dots \\ 0 \\ -(k11+k12) \cdot a^2 \\ 0 \\ -(k11+k12) \cdot a^2 \\ 0 \\ -(k12+k11) \cdot a^2 \\ 0 \\ -(k11+k12) \cdot a^2 \\ 0 \\ -(k11+k12) \cdot a^2 \\ 0 \\ -(k11+k12) \cdot a^2 \\ 0 \\ -I_p \cdot \omega \\ 0 \\ -I_p \cdot \omega \\ 0 \\ -(k11+k12) \cdot a^2 \\ 0 \\ -(k11+k12) \cdot a^2 \\ 0 \\ -(k11+k12) \cdot a^2 \\ 0 \\ -c1 \cdot a^2 \\ 0 \\ -c1 \cdot a^2 \end{matrix} $	$ \begin{matrix} Z_1 \\ Z_2 \\ \vdots \\ Z_5 \\ Z_6 \\ \theta_A \\ \theta_B \\ \theta_{rd} \\ \theta_{ps} \\ \vdots \\ \theta_{ps} \\ \theta_{ps} \\ \theta_{ps} \\ \theta_{ps} \\ \theta_{ps} \\ \theta_{ps} \\ y_1 \\ y_2 \\ \theta_2 \dots \theta_{34} \end{matrix} $	$ \begin{matrix} -k11 \cdot g11 - \dots - k12_y \cdot g12_y \\ k11 \cdot g11 + \dots + k12_y \cdot g12_y - W \cdot R - Fm \\ \vdots \\ (k11 \cdot g11 - k12_y \cdot g12_y) \cdot a \\ (k11_y \cdot g11_y - k12_y \cdot g12_y) \cdot a \\ (k12_y \cdot g12_y - k11_y \cdot g11_y) \cdot a \\ (k12_y \cdot g12_y - k11_y \cdot g11_y) \cdot a \end{matrix} $

$ \begin{matrix} 8k1+8k2+k11+\dots+k12_y \\ \vdots \\ 0 & 0 & -8k1 & 0 \end{matrix} $	$ \begin{matrix} 6k1 \cdot a^2 + 6k2 \cdot a^2 + \dots \\ 0 \\ -(k11+k12) \cdot a^2 \\ 0 \\ 6k1 \cdot b^2 + 6k2 \cdot b^2 + \dots \\ 0 \\ -(k11+k12) \cdot a^2 \\ 0 \\ -(k11+k12) \cdot a^2 \\ 0 \\ -(k12+k11) \cdot a^2 \\ 0 \\ -(k11+k12) \cdot a^2 \\ 0 \\ -(k11+k12) \cdot a^2 \\ 0 \\ -(k11+k12) \cdot a^2 \\ 0 \\ -I_p \cdot \omega \\ 0 \\ -I_p \cdot \omega \\ 0 \\ -(k11+k12) \cdot a^2 \\ 0 \\ -(k11+k12) \cdot a^2 \\ 0 \\ -(k11+k12) \cdot a^2 \\ 0 \\ -c1 \cdot a^2 \\ 0 \\ -c1 \cdot a^2 \end{matrix} $	$ \begin{matrix} Z_1 \\ Z_2 \\ \vdots \\ Z_5 \\ Z_6 \\ \theta_A \\ \theta_B \\ \theta_{rd} \\ \theta_{ps} \\ \vdots \\ \theta_{ps} \\ \theta_{ps} \\ \theta_{ps} \\ \theta_{ps} \\ \theta_{ps} \\ \theta_{ps} \\ y_1 \\ y_2 \\ \theta_2 \dots \theta_{34} \end{matrix} $
$ \begin{matrix} -k11 \cdot g11 - \dots - k12_y \cdot g12_y \\ k11 \cdot g11 + \dots + k12_y \cdot g12_y - W \cdot R - Fm \\ \vdots \\ (k11 \cdot g11 - k12_y \cdot g12_y) \cdot a \\ (k11_y \cdot g11_y - k12_y \cdot g12_y) \cdot a \\ (k12_y \cdot g12_y - k11_y \cdot g11_y) \cdot a \\ (k12_y \cdot g12_y - k11_y \cdot g11_y) \cdot a \end{matrix} $	$ \begin{matrix} -k11 \cdot g11 - \dots - k12_y \cdot g12_y \\ k11 \cdot g11 + \dots + k12_y \cdot g12_y - W \cdot R - Fm \\ \vdots \\ (k11 \cdot g11 - k12_y \cdot g12_y) \cdot a \\ (k11_y \cdot g11_y - k12_y \cdot g12_y) \cdot a \\ (k12_y \cdot g12_y - k11_y \cdot g11_y) \cdot a \\ (k12_y \cdot g12_y - k11_y \cdot g11_y) \cdot a \end{matrix} $	$ \begin{matrix} Z_1 \\ Z_2 \\ \vdots \\ Z_5 \\ Z_6 \\ \theta_A \\ \theta_B \\ \theta_{rd} \\ \theta_{ps} \\ \vdots \\ \theta_{ps} \\ \theta_{ps} \\ \theta_{ps} \\ \theta_{ps} \\ \theta_{ps} \\ \theta_{ps} \\ y_1 \\ y_2 \\ \theta_2 \dots \theta_{34} \end{matrix} $

(4.5)

At 0 rad/sec spin velocity of rotors, given the initial condition when the central 5 rotors are loaded on catcher bearings (Fig. 35) and the bump information listed in Table 5, the simulation result of relative motion between rotors and housings is shown in Fig. 36. As the spin velocity increases, gyroscopic effects would lead to large vibration and cause rotors bouncing between the upper and lower catcher bearings as shown in Fig. 37. In order to ensure the rotors would still sit on the lower catcher bearings during the bump, additional downward magnetic forces are applied. Fig. 38 shows the rotors and lower catcher bearings would keep contact even at high rate of spin when applying 20,000 lbs downward magnetic forces.

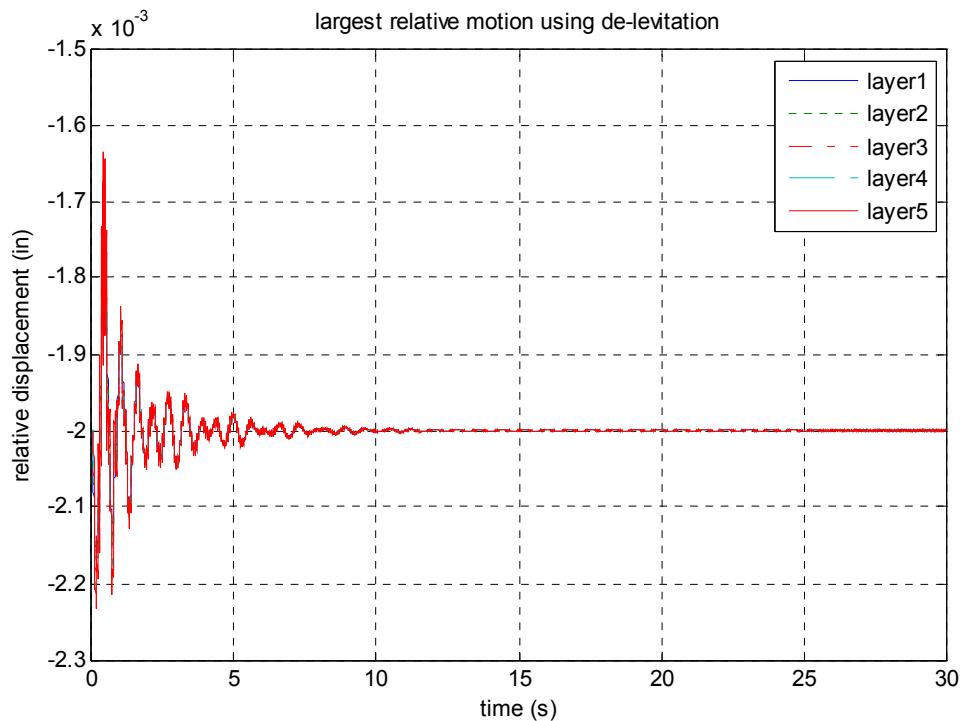


Fig. 36. De-levitation without downward magnetic force at 0 rad/sec spin rate

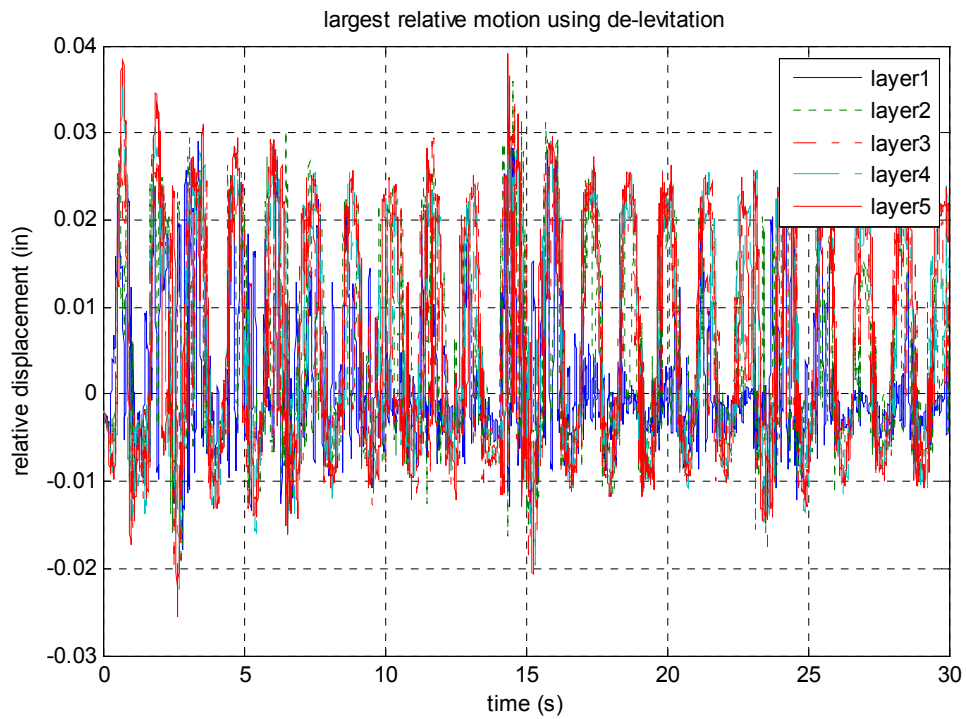


Fig. 37. De-levitation without downward magnetic force at rotors' spin velocity 500 rad/sec

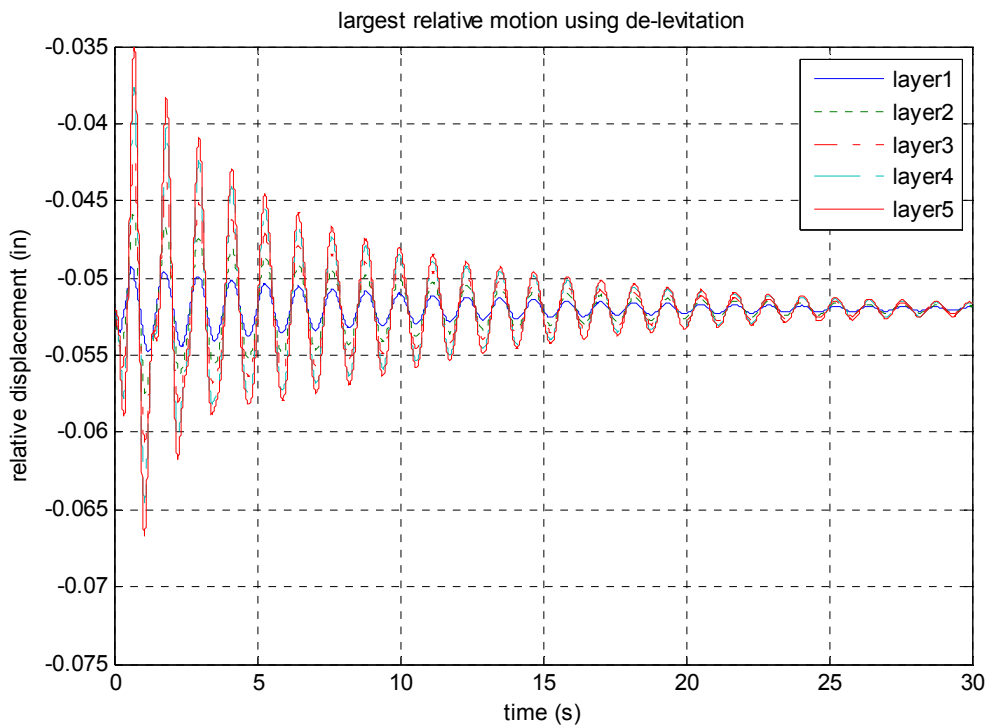


Fig. 38. De-levitation with 20,000lbs downward magnetic forces at spin velocity 500 rad/sec

Compared with the original method, de-levitation provides a means to protect not only AMBs, but also Catcher Bearings since the instant loading(shock) is almost removed. Furthermore, gyroscopic effects significantly reduced by using de-levitation method.

However, the limitation of implementing the de-levitation method should also be considered. There are mainly three problems using de-levitation. First, there are lots of bumps in reality. It is not practical to de-levitate the rotors everytime the train hits the bump. Second, by simulation, it is found that only with huge downward magnetic forces would the de-levitation method really work. In practice, it might be difficult to generate these huge forces. Third, catcher bearings might fail due to the huge and long-time service loading.

4.4 Model with gimbals

Since gyroscopic is the main impact of large vibrations during the bump, the ideal way is to remove the pitch motion input induced by the slug car floor(and gyro effect induced by the spinning rotor itself). The orientation of rotors would remain nearly fixed by using gimbals, regardless of any motion of the platform on which they are mounted. In this case, the flywheel system could be equipped with one-frame gimbal as shown in Fig. 39. The flywheel stack is supported by gimbal, which is used to prevent the θ_x floor input from transmitting to flywheel systems. As can be seen from Fig. 39, flywheel stack is supported by a shaft which can rotate freely through bearings on the stator.

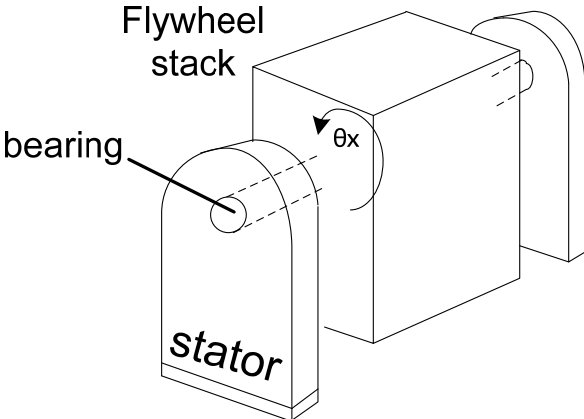


Fig. 39. Gimbal model

Fig. 40 shows the simulation results of original model without de-levitation when pitch motion input is removed. The rotors' spin rate is 500 rad/sec, the AMB stiffness is 250,000lbs/in.

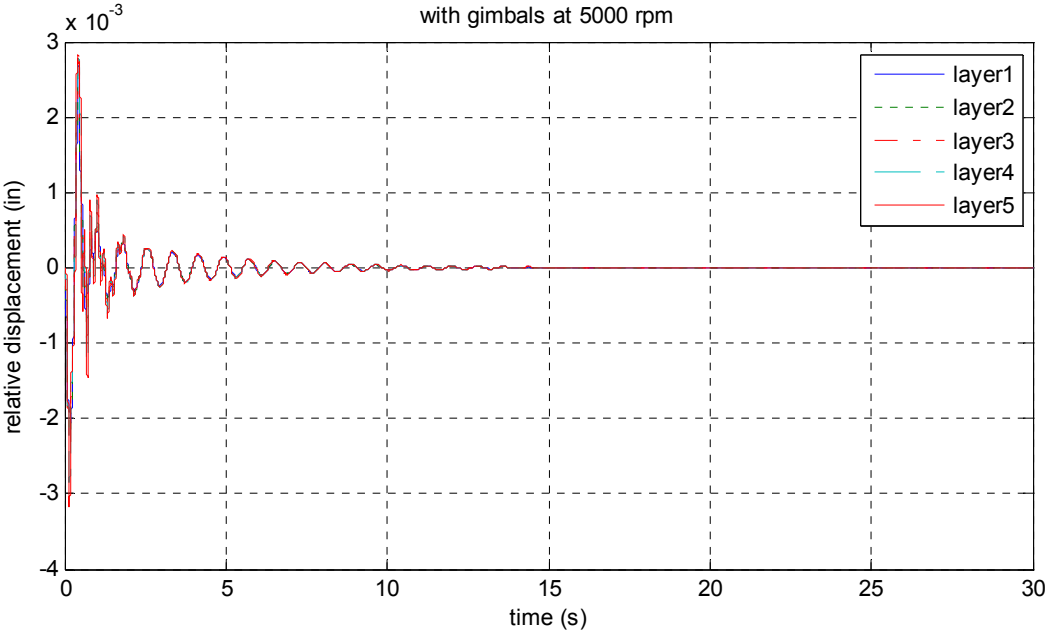


Fig. 40. Ramp input simulation with gimbals at spin rate 500 rad/sec

As predicted, the gyroscopic effects are suppressed by using gimbals. This can be an alternative method in practice, but the mechanical design and manufacturing might be more complicated.

Table 9 and 10 list the time to separate from catcher bearing with and without gimbals for different AMB stiffness. The result shows gimbals can not only suppress the gyroscopic effect, they also help decrease the rotor and catcher bearing's interactive time since the θ motion is removed by the gimbals. With gimbals, at AMB stiffness around 100,000 lbs/in, there is no contact between rotors and catcher bearings.

Table 9. Time to separate from catcher bearing for different AMB stiffness with gimbals

Time to separate from catcher bearing(CB) vs. K_{AMB} with gimbals	
AMB stiffness	Time to separate from CB
1,000 (lbs/in)	18 seconds
10,000 (lbs/in)	2.2 seconds
100,000 (lbs/in)	never touch CB (maximum relative displacement 0.008 inch)
250,000 (lbs/in)	never touch CB (maximum relative displacement 0.003 inch)

Table 10. Time to separate from catcher bearing for different AMB stiffness without gimbals

Time to separate from catcher bearing(CB) vs. K_{AMB} without gimbals	
AMB stiffness	Time to separate from CB
1,000,000 (lbs/in)	135 seconds
500,000 (lbs/in)	longer than 300 second
250,000 (lbs/in)	longer than 300 second
100,000 (lbs/in)	longer than 300 second

5. SUMMARY

- For sinusoidal floor input case:

The maximum relative displacement is 2.8e-6 inch at 10 Hz using the sinusoidal floor input profile given by Ahmadian and Venezia 2000. One of the critics is that, it is hard to believe such small displacement happens on the train floor according to personal experiences. The input vertical profile may not be accurate since it is reproduced from the reference paper. At low frequency range, the floor acceleration is fairly small (almost zero compared to the peak value). However, by assuming floor motion in the form of $z = A \cdot e^{i\omega t}$, then floor acceleration is in the form of $\ddot{z} = -A \cdot \omega^2 \cdot e^{i\omega t}$, converting these acceleration to displacement through dividing acceleration amplitude by corresponding frequency², the small acceleration amplitude in the low frequency may turn out to be significant in the displacement amplitude.

From AAR data listed in Table 4, there are indeed some peak displacements at low frequencies. By using the AAR data for sinusoidal floor input case(consider only vertical motion), the maximum relative displacement is 0.013 inch at AMB stiffness 1,000 lbs/in. At high AMB stiffness 250,000 lbs/in, the maximum relative displacement decreases significantly, about 6e-5 inch.

- For ramp support input case:

Table 11 lists a comparison for different methods.

Table 11. Comparison of different methods for ramp support input

	Max. relative motion:	Touch catcher bearing or not?	Oscillation time after bump?
without catcher bearings:	0.1 inch	—	Long-lasting
with catcher bearings:	within 0.02 inch	yes	Long-lasting
De-levitation: ($K_{\text{catcher brg.}}=1e8 \text{ lbs/in}$)	-0.0003~ -0.0007 inch	Always sit on lower catcher brg.	30-sec
With gimbals:	0.003 inch	no	10-sec

At 500 rad/sec spin rate, the maximum relative motion is up to 0.1 inch without catcher bearing, and there is long-lasting oscillation after the bump due to gyroscopic effect.

Then, catcher bearing is introduced to protect AMB from colliding with rotor. Maximum relative motion is limited within the allow gap between AMB and rotor, but there is still long-lasting oscillation happening after the bump due to gyroscopic effect.

One of the solutions to suppress this long-lasting oscillation is de-levitation. This method can ensure the contact between rotor and lower catcher bearings during the bump, and the oscillation is successfully suppressed.

Another solution is to equip gimbals to the flywheel system. By doing so, we exclude the disturbance of the pitch motion from floor. And it is found that, we can not only guarantee there is no contact between rotor and catcher bearing when the train goes through bumps with 1:150 slope, but there is almost no oscillation after bumps.

REFERENCES

- Ahmadian, M. and J. J. Venezia (2000). "An experimental evaluation of noise and vibrations in modern locomotive cabs." *Proc. of the 2000 ASME/IEEE Joint Railroad Conference*.
- Boyce, L., T. J. Kozik, and E. Parzen. (1984). "Probabilistic design and analysis of foundation forces for a class of unbalanced rotating machines." *ASME Journal of Vibration, Acoustics, Stress, and Reliability in Design*, 106(83): 90-99.
- Flex-bolt Sandwich Mounts. *Product Catalog, Lord Company*: 29-38.
- Gangadharan, K. V., C. Sujatha, and V. Ramamurti. (2008). "Dynamic response of railroad vehicles: a frequency domain approach." *Int. J. Heavy Vehicle Systems*, 15(1): 65-81.
- Ginsberg, J. H. (2001). *Mechanical and structural vibrations theory and applications*, John Wiley & Sons, New York.
- Kaul, M. K. (1978). "Spectrum-consistent time-history generation." *Journal of the Engineering Mechanics Division*, 104(4): 781-787.
- Nicks, J. (2009). "The bump at the end of the railway bridge." *Ph.D. Dissertation*, College Station, Texas, Texas A&M University.
- Park, J., A. Palazzolo, R. Tucker, and A. Kenny. (2008). "Locomotive flywheels to reduce NO_x emissions and fuel consumption." College Station, Texas, Texas A&M University: 5-7.
- Reiff, R. P. and J. Robeda (2003). "Simulating the vibration environment for locomotive-based friction control application systems." Pueblo, Colorado, Association of American Railroads.
- Shabana, A. A., K. E. Zaazaa, and H. Sugiyama. (2008). *Railroad vehicle dynamics*, CRC Press, Boca Raton, Fla.
- Singh, M. P. (1980). "Seismic response by SRSS for nonproportional damping." *Journal of engineering mechanics division, ASCE*, 106(6): 1405-1419.
- Singh, M. P. and S. L. Chu (1976). "Stochastic considerations in seismic analysis of structures." *Journal of Earthquake Engineering and Structural Dynamics*, 4: 295-307.

- Subbiah, R., R. B. Bhat, and T.S. Sankar. (1985). "Response of rotors subjected to random support excitations." *Journal of Vibration, Acoustics, Stress, and Reliability in Design*, 107: 453-459.
- Sun, Y. Q. and M. Dhanasekar (2002). "A dynamic model for the vertical interaction of the rail track and wagon system." *International Journal of Solids and Structures*, 39: 1337-1359.
- Thompson, D. J. (1993). "Wheel-rail noise generation, part 1: introduction and interaction model." *Journal of Sound and Vibration*, 161(3): 387-400.
- Vance, J. M. (1988). *Rotordynamics of turbomachinery*. Wiley, New York.

1289000900	0	-12500	0	-644508900	0	0	0	0	0	0	0	0	0	0	0	0	0	0	0	0	0	0	0	0	0	0		
0	1289000900	0	-12500	0	-644508900	0	0	0	0	0	0	0	0	0	0	0	0	0	0	0	0	0	0	0	0	0	0	
-12500	0	12500	0	0	0	0	0	0	0	0	0	0	0	0	0	0	0	0	0	0	0	0	0	0	0	0	0	
0	-12500	0	12500	0	0	0	0	0	0	0	0	0	0	0	0	0	0	0	0	0	0	0	0	0	0	0	0	
-644508900	0	0	1289000900	0	-12500	0	-644508900	0	0	0	0	0	0	0	0	0	0	0	0	0	0	0	0	0	0	0	0	
0	-644508900	0	0	1289000900	0	-12500	0	-644508900	0	0	0	0	0	0	0	0	0	0	0	0	0	0	0	0	0	0	0	
0	0	0	0	-12500	0	12500	0	0	0	0	0	0	0	0	0	0	0	0	0	0	0	0	0	0	0	0	0	
0	0	0	0	0	-12500	0	12500	0	0	0	0	0	0	0	0	0	0	0	0	0	0	0	0	0	0	0	0	
0	0	0	0	0	0	0	-644508900	0	0	1074194000	0	-12500	0	-429672600	0	859357700	0	-12500	0	-429672600	0	0	0	0	0	0	0	0
0	0	0	0	0	0	0	0	-644508900	0	0	1074194000	0	-12500	0	-429672600	0	859357700	0	-12500	0	-429672600	0	0	0	0	0	0	0
0	0	0	0	0	0	0	0	0	0	0	-12500	0	12500	0	0	0	0	0	0	0	0	0	0	0	0	0	0	0
0	0	0	0	0	0	0	0	0	0	0	0	-12500	0	12500	0	0	0	0	0	0	0	0	0	0	0	0	0	0
0	0	0	0	0	0	0	0	0	0	0	0	0	0	0	-12500	0	12500	0	0	0	0	0	0	0	0	0	0	0
0	0	0	0	0	0	0	0	0	0	0	0	0	0	0	0	-12500	0	12500	0	0	0	0	0	0	0	0	0	0
0	0	0	0	0	0	0	0	0	0	0	0	0	0	0	0	0	0	-12500	0	12500	0	0	0	0	0	0	0	0
0	0	0	0	0	0	0	0	0	0	0	0	0	0	0	0	0	0	0	0	-12500	0	12500	0	0	0	0	0	0
0	0	0	0	0	0	0	0	0	0	0	0	0	0	0	0	0	0	0	0	0	-12500	0	12500	0	0	0	0	0
0	0	0	0	0	0	0	0	0	0	0	0	0	0	0	0	0	0	0	0	0	0	-12500	0	12500	0	0	0	0
0	0	0	0	0	0	0	0	0	0	0	0	0	0	0	0	0	0	0	0	0	0	0	-12500	0	12500	0	0	0

$K_{\theta} =$

$$M = \begin{pmatrix} M_{z} & 0 & 0 & 0 \\ 0 & M_{\theta} & 0 & 0 \\ 0 & 0 & 0 & 0 \\ 0 & 0 & 0 & 0 \end{pmatrix}_{30 \times 30}, \quad C = \begin{pmatrix} C_{z} & 0 & 0 & 0 \\ 0 & C_{\theta} & 0 & 0 \\ 0 & 0 & 0 & 0 \\ 0 & 0 & 0 & 0 \end{pmatrix}_{30 \times 30}, \quad K = \begin{pmatrix} K_{z} & 0 & 0 & 0 \\ 0 & K_{\theta} & 0 & 0 \\ 0 & 0 & 0 & 0 \\ 0 & 0 & 0 & 0 \end{pmatrix}_{30 \times 30}$$

Spin velocity: 300 rad/sec

VITA

Xiaohua Zhang received his Bachelor of Engineering degree from Shanghai University, China. He has been a student worker in Vibration Control and Electromechanics Lab at Texas A&M since October, 2008. He plans to start his PhD study under the supervision of Dr. Palazzolo in the spring, 2010.

Mr. Zhang's permanent address is: Room 601, Entrance 2, Wenchangong middle lane No. 59, Leshan City, Sichuan Province, P. R. China, 614000. His email is zxhfi@neo.tamu.edu.